Root development is maintained by specific bacteria-bacteria interactions within a complex microbiome

Authors: Omri M. Finkel[1,2†], Isai Salas-González[1,2,3†], Gabriel Castrillo[1,2†‡], Theresa F. Law[1,2], Jonathan M. Conway[1,2], Paulo José Pereira Lima Teixeira[1,2¤], Corbin D. Jones[1,3,4,5,6,7], Jeffery L. Dangl[1,2,3,6,7,8*]

Affiliations:

[1]Department of Biology, University of North Carolina at Chapel Hill, Chapel Hill, North Carolina, United States of America.

[2]Howard Hughes Medical Institute, University of North Carolina at Chapel Hill, Chapel Hill, North Carolina, United States of America.

[3]Curriculum in Bioinformatics and Computational Biology, University of North Carolina at Chapel Hill, Chapel Hill, North Carolina, United States of America.

[4]Department of Genetics, University of North Carolina at Chapel Hill, Chapel Hill, North Carolina, United States of America.

[5]Lineberger Comprehensive Cancer Center, University of North Carolina at Chapel Hill, Chapel Hill, North Carolina, United States of America.

[6]Carolina Center for Genome Sciences, University of North Carolina at Chapel Hill, Chapel Hill, North Carolina, United States of America.

[7]Curriculum in Genetics and Molecular Biology, University of North Carolina at Chapel Hill, Chapel Hill, North Carolina, United States of America.

[8]Department of Microbiology and Immunology, University of North Carolina at Chapel Hill, Chapel Hill, North Carolina, United States of America.

*Correspondence to: dangl@email.unc.edu

†These authors contributed equally to this work.

‡Current address: Future Food Beacon of Excellence and the School of Biosciences, University of Nottingham, Sutton Bonington, United Kingdom

¤Current address: Department of Biology, “Luiz de Queiroz” College of Agriculture (ESALQ), University of São Paulo (USP), Piracicaba, São Paulo, Brazil

Abstract

Plants grow within a complex web of species interacting with each other and with the plant via a wide repertoire of chemical signals. To model plant-microbe-microbe-environment interactions, we inoculated seedlings with a defined 185-member bacterial synthetic community (SynCom), and manipulated the abiotic environment to enable classification of the SynCom to modules of co-occurring strains. We deconstructed the SynCom based on these modules, identifying a single bacterial genus, *Variovorax*, which reverts phenotypic effects on root development induced by a wide diversity of bacterial strains and by the entire 185-member community. *Variovorax* use mechanisms related to auxin and ethylene manipulation to balance this ecologically realistic root community's effects on root development. We demonstrate metabolic signal interference within a complex model community, defining *Variovorax* as determinants of bacteria-plant communication networks.

Introduction

Plant phenotypes, and ultimately fitness, are influenced by the microbes living in close association with them (*1*–*4*). This plant microbiota assembles based on plant-derived cues (*5*) resulting in myriad plant-microbe interactions. Beneficial and detrimental microbial effects on plants can be direct, via production of chemical signals (*6*, *7*) or modulation of nutrient availability (*1*, *4*, *8*); or they can be an indirect consequence of microbe-microbe interactions (*3*). A potentially significant class of microbe-microbe interactions is metabolic signal interference (*7*, *9*): rather than direct antagonism, microbes interfere with the delivery of chemical signals produced by other microbes, altering plant-microbe signaling (*10*–*12*).

Here, we apply a plant microbiota synthetic community (SynCom) to axenic plants, to ask how microbe-microbe interactions shape plant phenotypes. We used plant colonization patterns across 16 abiotic conditions to guide stepwise deconstruction of the SynCom, leading to the identification of a single bacterial genus that is required for maintaining the root's intrinsically controlled developmental program by tuning its chemical landscape.

Results

We established a controlled plant-microbiota microcosm representing the native bacterial microbiota on agar plates. We inoculated 7-day-old seedlings with a defined 185-member bacterial SynCom (fig. S1 and data S1) composed of genome-sequenced isolates obtained from

Arabidopsis roots (Material and Methods 1). To test the robustness of microbiota assembly to the abiotic environment, we exposed each microcosm to one of 16 different abiotic contexts by manipulating four variables (salinity, temperature, phosphate concentration and pH). We measured SynCom composition in root, shoot and agar fractions 12 days post-inoculation using 16S rRNA amplicon sequencing. Across all abiotic variables, fraction (agar, root, shoot; fig. S2) explained most (40%) of the variance. Abiotic conditions significantly affected both alpha- (fig. S3) and beta-diversity (Fig. 1A). Our SynCom therefore exhibits deterministic niche sorting within the plant across a range of abiotic conditions.

We calculated pairwise correlations in relative abundance across all samples, and identified four well-defined modules of co-occurring strains (A, B, C and D; Fig. 1B and data S2). These modules formed distinct phylogenetically-structured guilds in association with the plant: module A contained mainly Gammaproteobacteria and was predominantly more abundant in the agar than in the seedling; module B contained mainly low-abundance Firmicutes, with no significant seedling enrichment trend; modules C and D were composed mainly of Alphaproteobacteria and Actinobacteria, respectively, and showed seedling-enrichment across all abiotic conditions (Figure 1A and data S2). Both Alphaproteobacteria (module C) and Actinobacteria (module D) are consistently plant-enriched across plant species (*13*), suggesting that they contain plant-association traits that are deeply rooted in their evolutionary histories.

We next asked whether the different modules of co-occurring strains play different roles in determining plant phenotypes (Materials and Methods 2). We inoculated seedlings with SynComs composed of modules A, B, C and D singly, or with all six possible pairwise module combinations (Fig. 2A), and imaged the seedlings 12 days post-inoculation. We observed strong primary root growth arrest in seedlings inoculated with plant-enriched modules C or D (Fig. 2A). This root growth inhibition (RGI) did not occur in seedlings inoculated with modules A or B, which do not contain plant-enriched strains (Fig. 2A, 2C and data S3). To test whether plant-enrichment and RGI are correlated traits, we inoculated seedlings in mono-association with each of the 185 SynCom members (Materials and Methods 3). Surprisingly, we observed that RGI-inducing strains were found in all four modules (Fig. 2B, fig. S4-S5 and data S4). Thus, in line with (*4*), plant-enrichment within a bacterial community does not predict phenotypic effects on seedlings in mono-association.

The mono-association assay confirmed that RGI is a prevalent trait across the plant bacterial microbiota. Thirty-four taxonomically diverse strains, derived from all four modules, induced RGI. However, neither the full SynCom nor derived SynComs of modules A or B exhibited RGI (Fig. 2A), suggesting that microbe-microbe interactions are responsible for RGI attenuation within these SynComs. Furthermore, in seedlings inoculated with module pairs, we observed an epistatic interaction: in the presence of module A, RGI caused by modules C and D was reverted (Fig. 2A). Thus, through deconstructing the SynCom into four modules, we found that bacterial effects on root development are governed by multiple levels of microbe-microbe interactions, exemplified by at least four instances: within modules A and B and between module A and modules C and D. Since three of these interactions involve module A, we predicted that this module contains strains that strongly attenuate RGI, preserving stereotypic root development.

To identify strains within module A responsible for intra- and inter-module RGI attenuation, we reduced our system to a tripartite plant-microbe-microbe system (Materials and Methods 4). We individually screened the 18 non-RGI strains from module A for their ability to attenuate RGI caused by representative strains from all four modules. We found that all strains from a single genus, *Variovorax* (Family Comamonadaceae) suppressed RGI caused by representative RGI-inducing strains from module C (*Agrobacterium* MF224) and module D (*Arthrobacter* CL28; Fig. 2D, fig. S6 and data S5). The strains from modules A (*Pseudomonas* MF48) and B (*Bacillus* MF107), were not suppressed by *Variovorax*, but rather by two closely related *Burkholderia* strains (CL11, MF384). A similar pattern was observed when we screened three selected RGI-suppressor *Variovorax* strains (CL14, MF160) and *Burkholderia* CL11, against a diverse set of RGI-inducers. *Variovorax* attenuated 13 of the 18 RGI-inducers tested (Fig. 2E-F, fig. S6 and data S6).

We further tested if our RGI-suppressor strains maintain their capacity to attenuate RGI in the context of the full 185-member community (Materials and Methods 5). We compared the root phenotype of seedlings exposed to either the full SynCom or to the same community dropping-out all ten *Variovorax* strains and/or all six *Burkholderia* strains (drop-out system, Fig. 3A-C). We found that *Variovorax* are necessary and sufficient to revert RGI within the full community (Fig. 3B-C and data S7). This result was robust across a range of biotic and abiotic contexts (Fig. 3D-E, fig. S7-S8 and data S7; Materials and Methods 6-7).

100 To ascertain the phylogenetic breadth of the *Variovorax* ability to attenuate RGI, we tested
101 additional *Variovorax* strains from across the genus' phylogeny (fig. S9A and data S1; Materials
102 and Methods 8). All tested *Variovorax* reverted RGI induced by *Arthrobacter* CL28 (Materials and
103 Methods 9). A strain from the nearest plant-associated outgroup to this genus, *Acidovorax*
104 Root219, did not revert RGI (fig. S9A-B and data S8). *Variovorax*-mediated RGI attenuation
105 extended to tomato seedlings, where *Variovorax* CL14 reverted *Arthrobacter* CL28-mediated RGI
106 (fig. S10, data S9, Materials and Methods 10). Thus, a single bacterial genus, *Variovorax,*
107 interacts with a wide diversity of bacteria to enforce stereotypic root development within complex
108 communities, independent of biotic or abiotic contexts, and this ability is general to this genus.
109
110 We tested whether *Variovorax* attenuate RGI by inhibiting growth of RGI-inducing strains
111 (Materials and Methods 11). We counted colony forming units of the RGI inducer *Arthrobacter*
112 CL28 from roots in the presence or absence of *Variovorax* CL14 and found that CL28 abundance
113 increased in the presence of *Variovorax* CL14 (fig. S11, data S10). To test whether *Variovorax*
114 modulates bacterial abundances in the whole community, we compared the bacterial relative
115 abundance profiles in seedlings colonized with the full SynCom to that colonized with the
116 *Variovorax* drop-out community (Materials and Methods 6d). We found no changes in the
117 abundances of RGI-inducing strains in response to the *Variovorax* drop-out (Fig. 3F). In fact,
118 *Variovorax* account for <1% of the community on our roots (Fig. 3G), and in natural soils (fig.
119 S12). Notably, while rare, *Variovorax* are root-enriched in two natural soils tested (fig. S12). These
120 results rule out the possibility that *Variovorax* enforce root developmental patterns by
121 antagonizing or outcompeting RGI-inducers. We hypothesized that RGI attenuation by *Variovorax*
122 is likely mediated by signal interference.
123
124 To study the mechanisms underlying RGI and RGI attenuation, we analyzed the transcriptomes
125 of seedlings colonized for 12 days with the RGI-inducer *Arthrobacter* CL28 and the RGI-attenuator
126 *Variovorax* CL14, either in mono-association with the seedling or in a tripartite combination (Fig.
127 2F; Materials and Methods 12). We also performed RNA-Seq on seedlings colonized with the full
128 SynCom (no RGI) or the *Variovorax* drop-out SynCom (RGI; Fig. 3A). Eighteen genes were
129 significantly induced only under RGI conditions across both experiments (Fig. 4A-B and data
130 S11). Seventeen of these are co-expressed genes related to the root apex (*14*) (Fig 4B and fig.
131 S13). The remaining gene is Indole-3-acetic acid-amido synthetase GH3.2, which conjugates
132 excess amounts of the plant hormone auxin and is a robust marker for late auxin responses (*15*,
133 *16*) (Fig. 4C). Production of auxins is a well-documented mechanism by which bacteria modulate

134 plant root development (*10*). Indeed, the top 12 auxin-responsive genes from an RNA-Seq study
135 examining acute auxin response in Arabidopsis (*15*) exhibited an average transcript increase in
136 seedlings exposed to our RGI-inducing conditions (Fig. 4C and data S12).

137

138 Next, we asked whether RGI-attenuation by *Variovorax* is directly and exclusively related to auxin
139 signaling (Materials and Methods 13). Besides auxin, other small molecules cause RGI. These
140 include the plant hormones ethylene (*17*) and cytokinin (*18*); and microbial-associated molecular
141 patterns (MAMPs) including the flagellin-derived peptide flg22 (*19*). We tested the ability of
142 diverse *Variovorax* strains and of the *Burkholderia* strain CL11 to revert RGI induced by auxins
143 (Indole-3-acetic acid [IAA] and the auxin analogue 2,4-Dichlorophenoxyacetic acid [2,4-D]),
144 ethylene (the ethylene precursor 1-Aminocyclopropane-1-carboxylic acid [ACC]), cytokinins
145 (Zeatin, 6-Benzylaminopurine) and flg22 peptide (fig. 4D). All tested *Variovorax* suppress RGI
146 induced by IAA or ACC (Figure 4D and data S13), with the exception of *Variovorax* YR216 which
147 did not suppress ACC-induced RGI and does not contain an ACC deaminase gene (fig. S9A), a
148 plant growth-promoting feature associated with this genus (*17*). *Burkholderia* CL11 was only able
149 to partially revert ACC-induced RGI. None of the *Variovorax* attenuated RGI induced by 2,4-D, by
150 flg22 or by cytokinins, indicating that *Variovorax* revert RGI induction by interfering with auxin
151 and/or ethylene signaling. Furthermore, this function is mediated by recognition of auxin by the
152 bacteria and not by the plant auxin response *per se* since RGI induced by 2,4-D is not reverted.
153 Indeed, we found that *Variovorax* CL14 degrades IAA *in-vitro* (fig. S14; Materials and Methods
154 14) and quenches fluorescence of the Arabidopsis auxin reporter line *DR5::GFP* caused by the
155 RGI inducer *Arthrobacter* CL28 (Fig. 4E, fig. S15 and data S14; Materials and Methods 15).

156

157 We used the auxin-insensitive *axr2-1* mutant (*20*), combined with a competitive inhibitor of
158 ethylene receptors, 1-Methylcyclopropene (1-MCP) (*21*), to examine the roles of plant auxin and
159 ethylene perception in bacterially-induced RGI (Materials and Methods 16). We inoculated wild
160 type seedlings and the *axr2-1* mutants, treated or not with 1-MCP, with the RGI-inducing
161 *Arthrobacter* CL28 or the *Variovorax* drop-out SynCom. We observed in both cases that bacterial
162 RGI is reduced in *axr2-1* and 1-MCP-treated wild type seedlings, and is further reduced in doubly-
163 insensitive 1-MCP-treated *axr2-1* seedlings, demonstrating a synergistic effect of auxin and
164 ethylene (Fig. 4F and data S15) on bacterial RGI. Thus, a complex SynCom can induce severe
165 morphological changes in root phenotypes via both auxin- and ethylene-dependent pathways,
166 and both are reverted when *Variovorax* are present. We conclude that seedlings growing in a
167 realistically diverse bacterial microbiota depend on specific taxa for maintaining a controlled

168 developmental program by tuning the root's response to its microbially-encoded chemical
169 landscape.
170
171 **Discussion**
172 Microbes communicate with the plant and each other by secreting a wide repertoire of secondary
173 metabolites, which have profound effects on plant physiology and development (*10*, *19*). Equally
174 important are the interactions between these signals, as in the case of quorum quenching (*12*) or
175 degradation of MAMPs (*22*). The degradation of bacterially-produced auxin is prevalent in the
176 rhizosphere, including among *Variovorax* (*10*, *11, 23*), but its consequences for the plant have
177 not been demonstrated in a community context. Intriguingly, sequenced *Variovorax* genomes do
178 not contain any canonical auxin degradation operons (Materials and Methods 18) (*23*), suggesting
179 a novel mechanism. This work demonstrates metabolic signal interference from within a complex
180 model community and stages *Variovorax* as key players in bacteria-plant communication
181 networks, demonstrating an ability to block bacterial effects on root development across a wide
182 range of biotic and abiotic contexts.
183
184 Signaling molecules and other secondary metabolites are products of evolution towards
185 increasing complexity that allows microbes to survive competition for primary metabolites. Our
186 results illuminate the importance of an additional trophic layer of microbes that utilize these
187 secondary metabolites for their own benefit, while providing the unselected exaptation (*24*) of
188 metabolic signal interference between the bacterial microbiota and the plant host. This potential
189 exaptation, and the consequent homeostasis of plant hormone signals that emerges from it,
190 allows the plant to maintain its root developmental program within a chemically rich matrix.
191 Moreover, our data suggest that *Variovorax* accomplish this function while not disrupting the
192 colonization of other taxa, some of which likely provide the host additional ecosystem services.
193 As we proceed to design and develop plant probiotics, we need to consider the maintenance of
194 intra-and inter-taxa microbial homeostasis as potential contributors to satisfactory invasion and
195 persistence of probiotic strains into standing heterogeneous microbial communities.

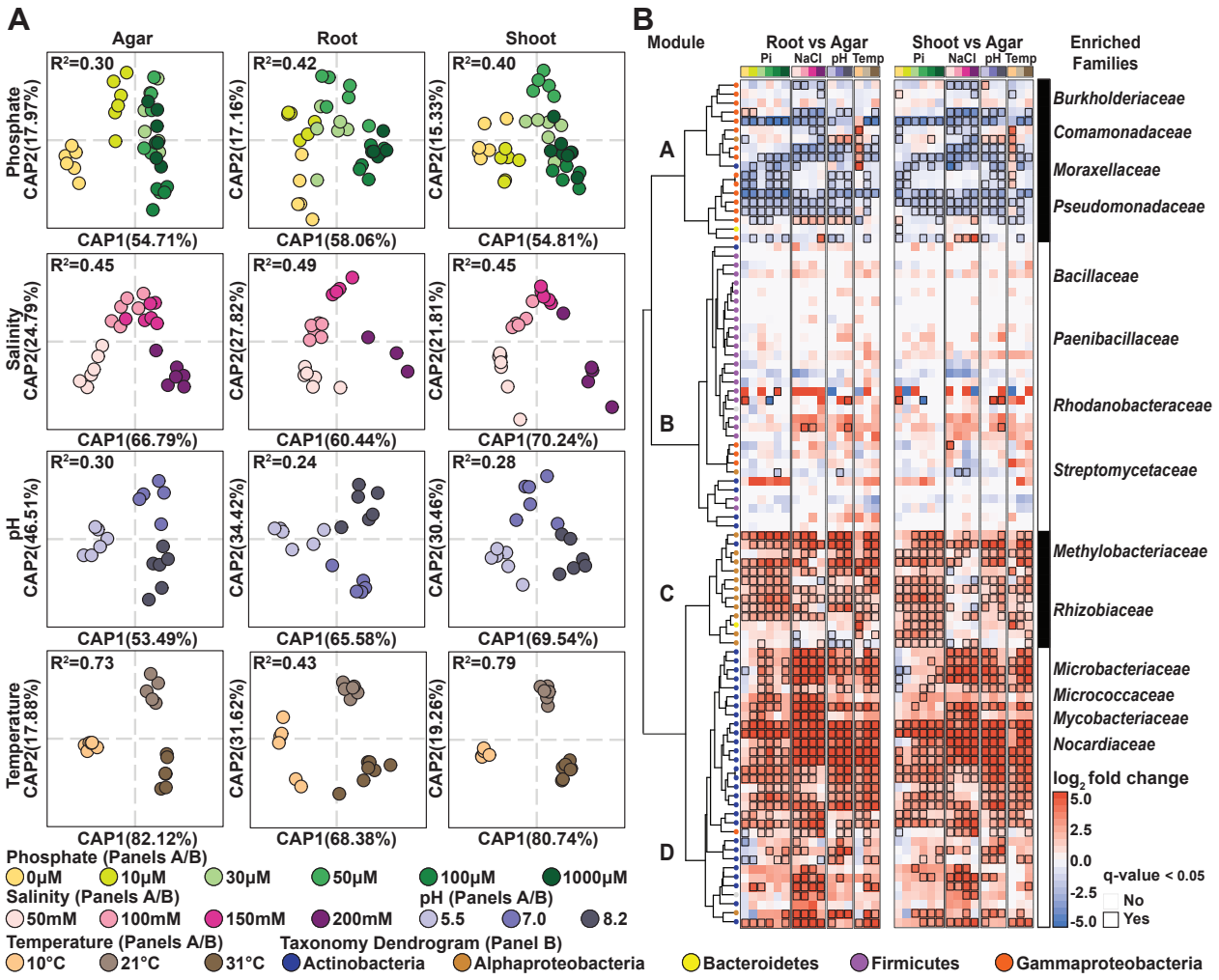

Fig. 1. Reproducible effects of abiotic conditions on the synthetic community assembly.

(A) Canonical analysis of principal coordinates (CAP) scatterplots showing the influence of each of the four abiotic gradients (phosphate, salinity, pH, temperature) within agar, root and shoot fractions. PERMANOVA R^2 values are shown within each plot. **(B)** Fraction enrichment patterns of the SynCom across abiotic gradients. Each row represents a USeq. Letters on the dendrogram represent the four modules of co-occurring strains (A, B, C, D). Dendrogram tips are colored by taxonomy. The heatmaps are colored by log2 fold changes derived from a fitted GLM. Positive fold changes (red gradient) represent enrichments in plant tissue (root or shoot) compared with agar, negative fold changes (blue gradient) represent depletion in plant tissue compared with agar. Comparisons with q-value < 0.05 are contoured in black. Family bar highlights enriched families within each module.

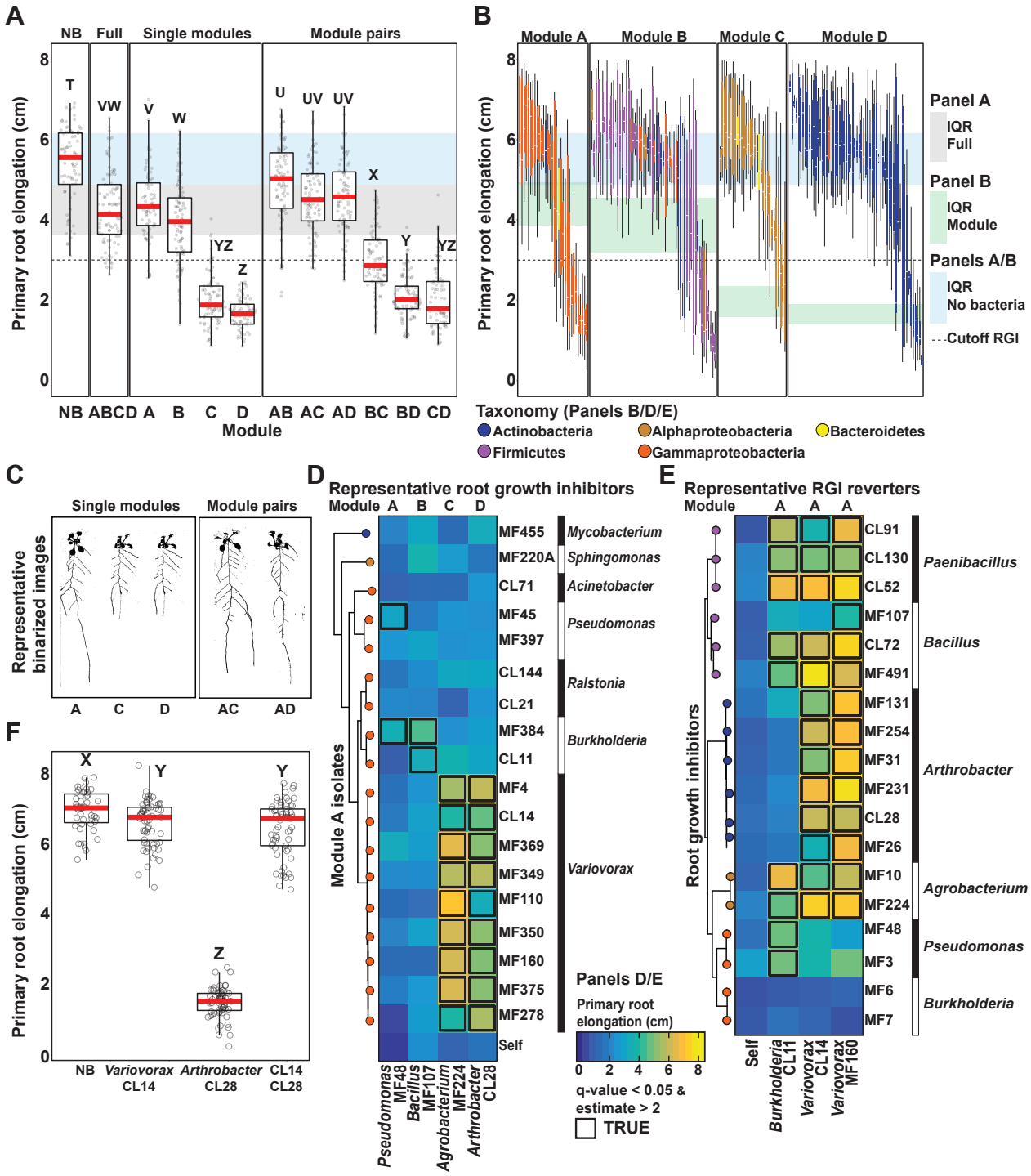
A
NB
Full
Single modules
Module pairs
Primary root elongation (cm)
T
VW
V
W
YZ
Z
U
UV
UV
X
Y
YZ
NB ABCD A B C D AB AC AD BC BD CD
Module
B
Module A
Module B
Module C
Module D
Panel A
IQR
Full
Panel B
IQR
Module
Panels A/B
IQR
No bacteria
Cutoff RGI
Taxonomy (Panels B/D/E)
Actinobacteria
Alphaproteobacteria
Bacteroidetes
Firmicutes
Gammaproteobacteria
C
Single modules
Module pairs
Representative binarized images
A C D AC AD
D
Representative root growth inhibitors
Module A B C D
Module A isolates
MF455
MF220A
CL71
MF45
MF397
CL144
CL21
MF384
CL11
MF4
CL14
MF369
MF349
MF110
MF350
MF160
MF375
MF278
Self
Mycobacterium
Sphingomonas
Acinetobacter
Pseudomonas
Ralstonia
Burkholderia
Variovorax
Pseudomonas MF48
Bacillus MF107
Agrobacterium MF224
Arthrobacter CL28
Panels D/E
Primary root elongation (cm)
0 2 4 6 8
q-value < 0.05 &
estimate > 2
TRUE
E
Representative RGI reverters
Module A A A
Root growth inhibitors
CL91
CL130
CL52
MF107
CL72
MF491
MF131
MF254
MF31
MF231
CL28
MF26
MF10
MF224
MF48
MF3
MF6
MF7
Paenibacillus
Bacillus
Arthrobacter
Agrobacterium
Pseudomonas
Burkholderia
Self
Burkholderia CL11
Variovorax CL14
Variovorax MF160
F
Primary root elongation (cm)
X
Y
Y
Z
NB
Variovorax CL14
Arthrobacter CL28
CL14 CL28

Fig. 2. Arabidopsis root length is governed by multiple bacteria-bacteria interactions within a community.

(A) Primary root elongation of seedlings grown with no bacteria (NB), with the full 185-member SynCom (Full) or with its subsets: Modules A, B, C and D alone (single modules), as well as all six possible pairwise combination of modules (module pairs). Differences between treatments are denoted using the compact letter display. **(B)** Primary root elongation of seedlings inoculated with single bacterial isolates. Isolates are colored by taxonomy and grouped by module membership. The strips across the panels correspond to the interquartile range (IQR) as noted at far right. The dotted line represents the cutoff used to classify isolates as root growth inhibiting (cutoff RGI). **(C)** Binarized image of representative seedlings inoculated with modules A, C and D, and with module combinations AC and AD. **(D, E)** Heatmaps colored by average primary root elongation of seedlings inoculated with different pairs of bacterial isolates: **(D)** with four representative RGI-inducing strains from each module (columns) alone (Self) or in combination with isolates from module A (rows), **(E)** with eighteen RGI-inducing strains (rows) alone (Self) or in combination with *Burkholderia* CL11, *Variovorax* CL14 or *Variovorax* MF160 (columns). Statistically significant RGI reversions are contoured in black. **(F)** Primary root elongation of uninoculated seedlings (NB) or seedlings inoculated with *Arthrobacter* CL28 and *Variovorax* CL14 isolates individually or jointly. Letters indicate post-hoc significance.

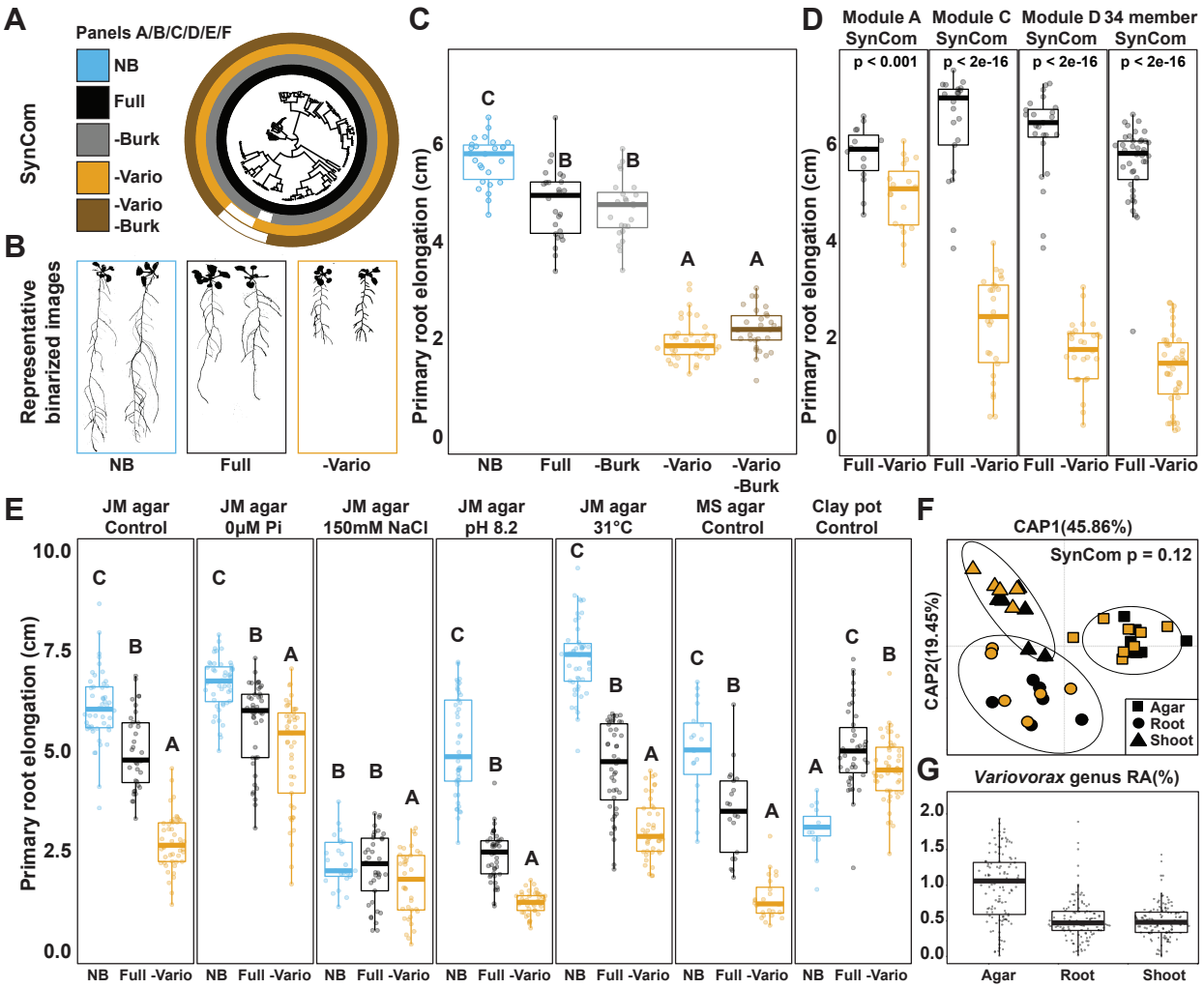

Fig. 3 *Variovorax* are necessary and sufficient to maintain stereotypic root development.

(A) Phylogenetic tree of 185 bacterial isolates. Concentric rings represent isolate composition of each SynCom treatment (-Burk: *Burkholderia* drop-out, -Vario: *Variovorax* drop-out). **(B)** Binarized image of representative uninoculated seedlings (NB), or seedlings with the full SynCom (Full) or the *Variovorax* drop-out SynCom (-Vario) treatments. **(C)** Primary root elongation of uninoculated seedlings (NB) or seedlings with the different SynCom treatments. **(D)** Primary root elongation of seedlings inoculated independently with four compositionally different SynComs (Module A, C, D and 34-member) with (Full) or without (Vario) 10 *Variovorax* isolates. FDR-corrected p-values are shown within each plot. **(E)** Primary root elongation of uninoculatd seedlings (NB), or seedlings with the Full SynCom or with the *Variovorax* drop-out SynCom (-Vario) across different abiotic conditions: unamended medium (JM agar control), phosphate starvation (JM agar 0 μM Pi), salt stress (JM agar 150 mM NaCl), high pH (JM agar pH 8.2) and high temperature (JM agar 31˚ C) and media: Johnson Medium (JM agar control), Murashige and Skoog (MS agar control) and calcined clay (Clay pot control). Letters indicate statistical significance. **(F)** Canonical analysis of principal coordinates scatterplots comparing community full vs *Variovorax* drop-out SynComs across all fractions (agar, root, shoot). PERMANOVA p-value is shown. **(G)** Relative abundance (RA) of the *Variovorax* genus within the full SynCom across the agar, root and shoot fractions.

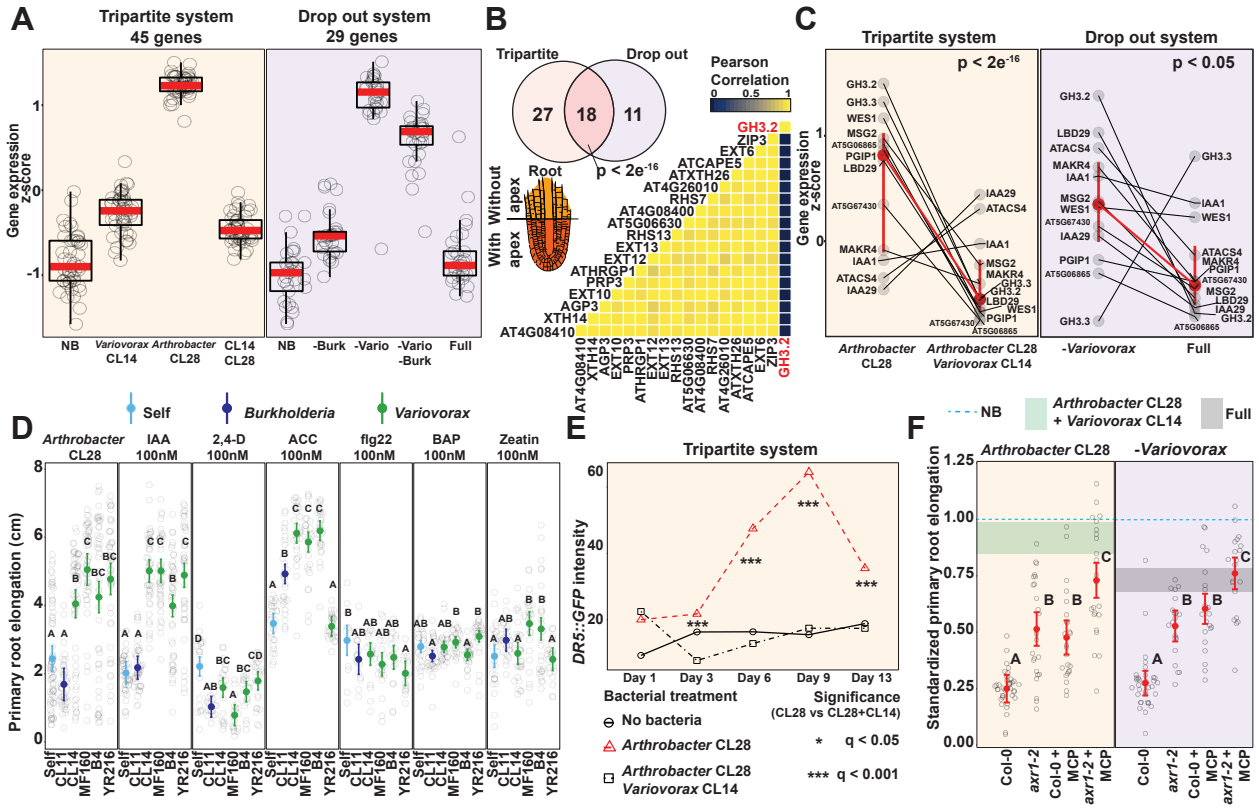

Fig. 4. *Variovorax* attenuation of root growth inhibition is related to auxin and ethylene signaling.

(A) Boxplots showing the average standardized expression of genes induced in seedlings in response to: Left (Tripartite system) *Arthrobacter* CL28 compared with uninoculated seedlings (NB) or seedlings inoculated with both *Arthrobacter* CL28 and *Variovorax* CL14 (CL14 CL28). Right (Drop-out System) Variovorax drop-out SynCom (-Vario) compared to uninoculated seedlings (NB) and to the full SynCom (Full). **(B)** Venn diagram showing the overlap in enriched genes between the tripartite and drop-out systems. The heatmap shows the pairwise correlation in expression of these 18 genes across tissues (14). **(C)** Standardized expression of 12 late-responsive auxin genes across the tripartite and drop-out systems. Each dot represents a gene. Identical genes are connected between bacterial treatments with a black line. Mean expression (95% CI intervals) of the aggregated 12 genes in each treatment is highlighted in red and connected between bacterial treatments with a red line. **(D)** Primary root elongation of seedlings grown with six hormone or MAMP RGI treatments (panels) individually (Self) or with either *Burkholderia* CL11 or four *Variovorax* isolates. Significance between the bacterial treatments is shown using the confidence letter display. **(E)** GFP intensity of *DR5::GFP* Arabidopsis seedlings grown with no bacteria, *Arthrobacter* CL28 and *Arthrobacter* CL28+*Variovorax* CL14. Significance within time points is denoted with asterisks. **(F)** Primary root elongation, standardized to sterile conditions, of wild type (Col-0) auxin unresponsive (*axr1-2*), ethylene unresponsive (Col-0 + MCP), or auxin/ethylene unresponsive (*axr1-2* + MCP) seedlings inoculated with RGI-inducing *Arthrobacter* CL28 or the *Variovorax* dropout SynCom (-*Variovorax*). The blue dotted line marks the relative mean length of uninoculated seedlings. The horizontal shade in each panel corresponds to the interquartile range of seedlings (all genotypes) grown with: *Arthrobacter CL28*+-*Variovorax* CL14), or the full 185-member SynCom including 10 *Variovorax* isolates (Full SynCom). Differences between treatments are denoted using the compact letter display.

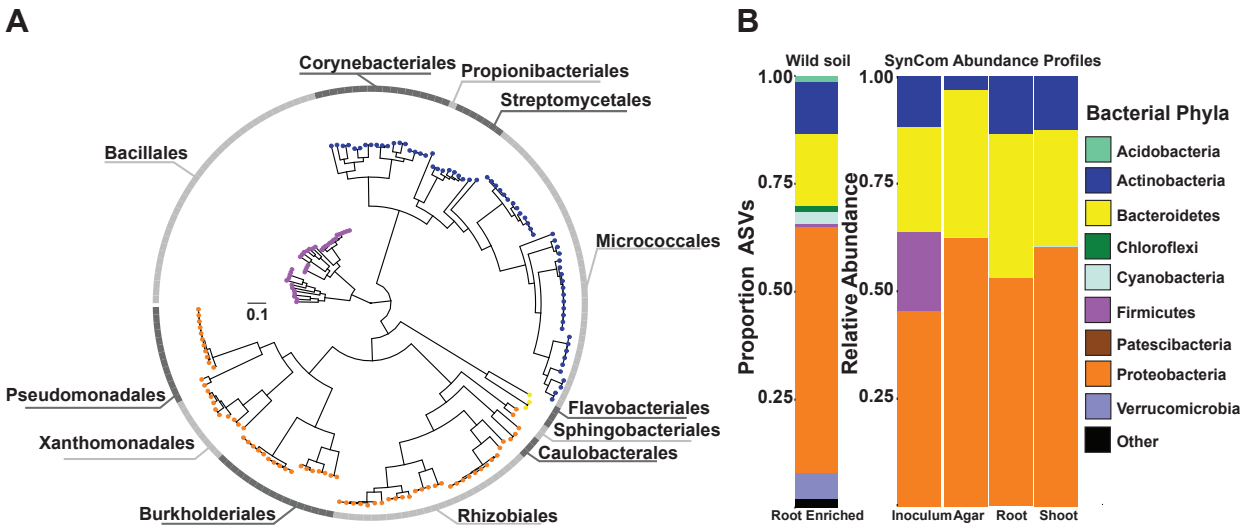

Fig. S1.
Synthetic community resembles the taxonomic makeup of natural communities. **(A)** Phylogenetic tree of 185 bacterial genomes included in the synthetic community (SynCom). The tree tips are colored according to phylum. The outer ring shows the distribution of the 12 distinct bacterial orders present in the SynCom. **(B)** The panel on the left (wild soil) shows the proportion of amplicon sequence variants (ASVs) enriched (q-value < 0.1) in the plant root in comparison to soil in a microbiota profiling study from the same soil that SynCom strains were isolated from (2). In the panel, ASVs are colored according to phylum. The panel on the right (SynCom panel) represents the relative abundance profiles of bacterial isolates across the initial inoculum, planted agar, root and shoot in plant exposed to the full SynCom. Bacterial isolates in the SynCom are colored based on their phylum.

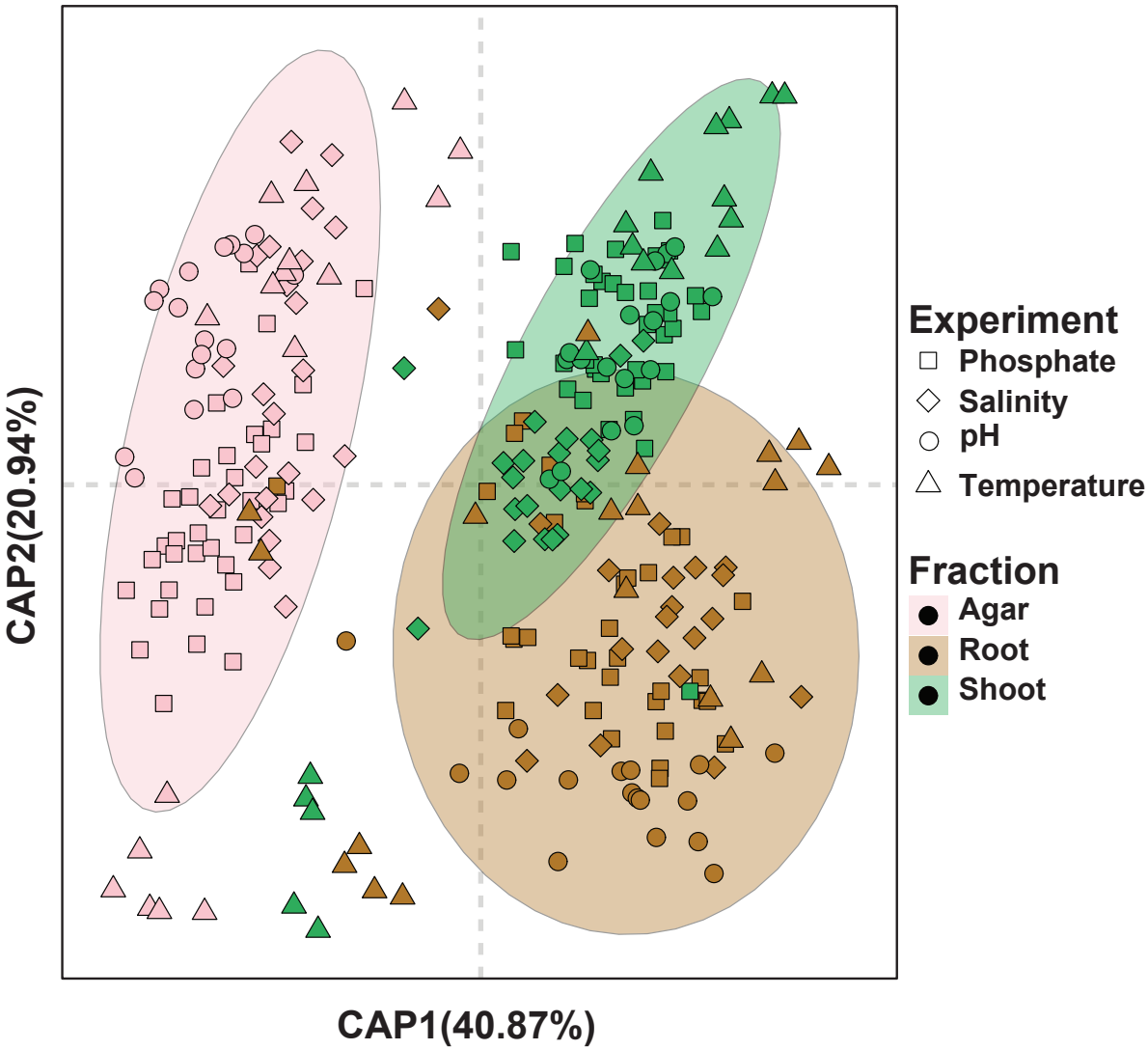

Fig. S2.
Plant microbiota assembly is robust to environmental variations.
Canonical analysis of principal coordinates showing the influence of the fraction (agar, root, shoot) on the assembly of the bacterial synthetic community across the four gradients used in this work (phosphate, salinity, pH, temperature). Different colors differentiate between the fractions and different shapes differentiate between experiments. Ellipses denote the 95% confidence level of each fraction.

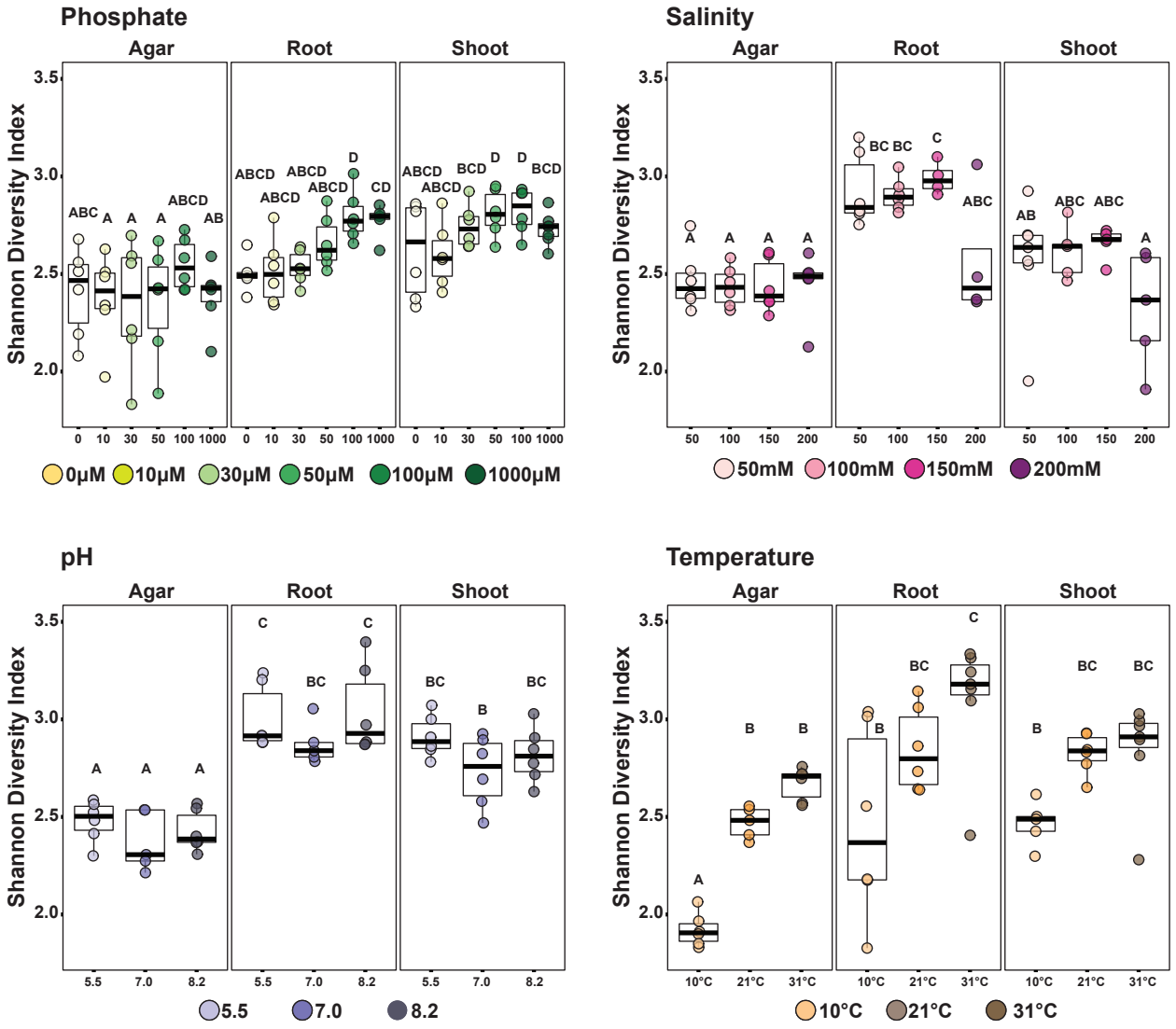

Fig. S3.

Abiotic conditions displayed reproducible effects on alpha-diversity.

Each panel represents the bacterial alpha-diversity across the different gradient conditions (phosphate, salinity, pH, temperature) and the fractions (agar, root, shoot) used in this work. Bacterial alpha-diversity was estimated using Shannon Diversity. Letters represent the results of the post hoc test of an ANOVA model testing the interaction between fraction and abiotic condition.

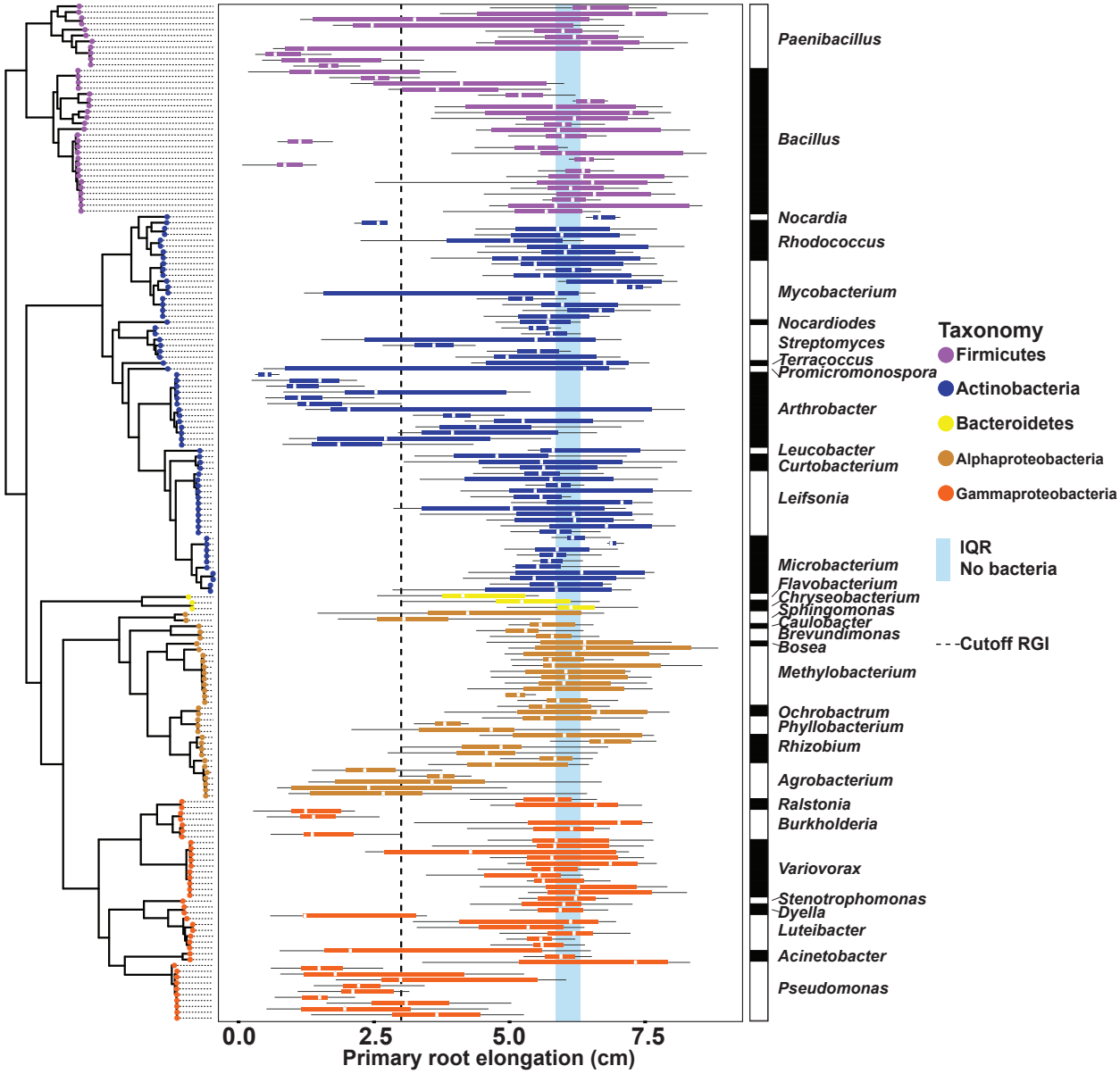

Fig. S4.

Root growth inhibition trait is distributed across bacterial phylogeny.

Primary root elongation of plants inoculated with single bacterial isolates (one boxplot per isolate). Isolates are ordered according to the phylogenetic tree on the left side of the panel and colored based on their genome-based taxonomy. The vertical blue strips across the panel corresponds to the interquartile range (IRQ) of plants grown in sterile conditions. The vertical dotted line represents the 3 cm cutoff used to classify strains as root growth inhibiting strains. The bar on the right side of the panel denotes the genus classification of each isolate.

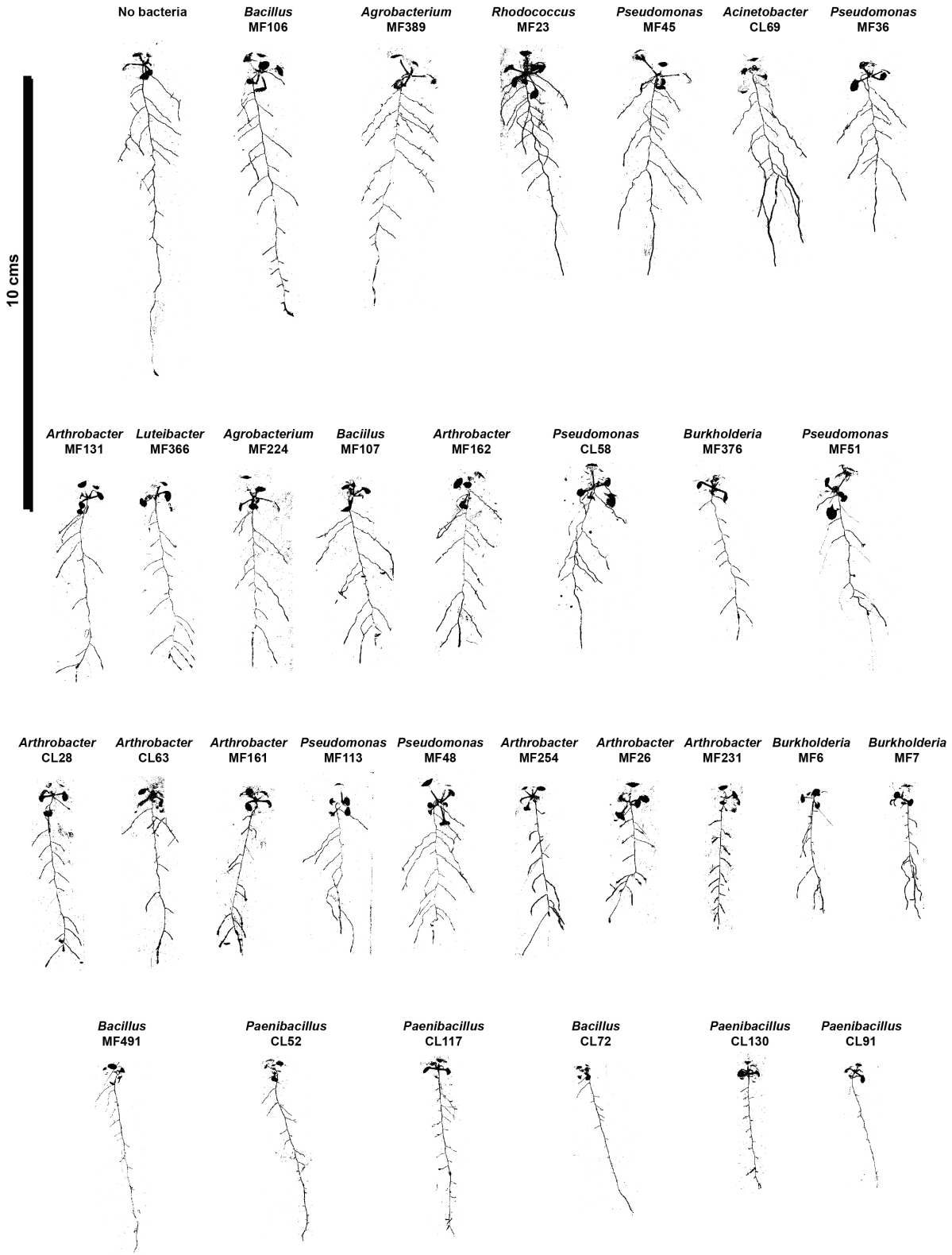

Fig. S5.

Root growth inhibition phenotypes comprise variable root architectures.

Binarized image of representative seedlings grown axenically (no bacteria) or with thirty-four root growth inhibiting (RGI) strains individually.

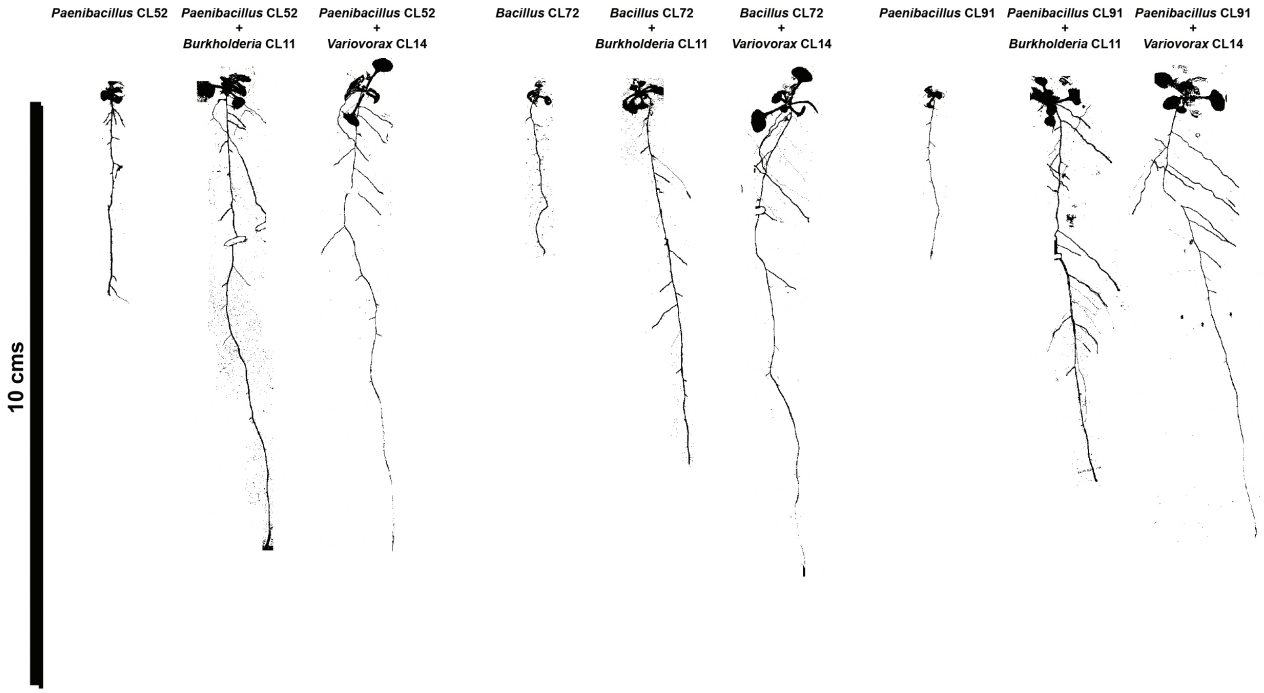

Fig. S6.
Example of strains that attenuate severe root and growth inhibition phenotypes.
Binarized image of representative seedlings grown with three severely growth inhibiting isolates (*Paenibacillus* CL52, *Bacillus* CL72 and *Paenibacillus* CL91) individually or jointly with *Burkholderia* CL11 or *Variovorax* CL14.

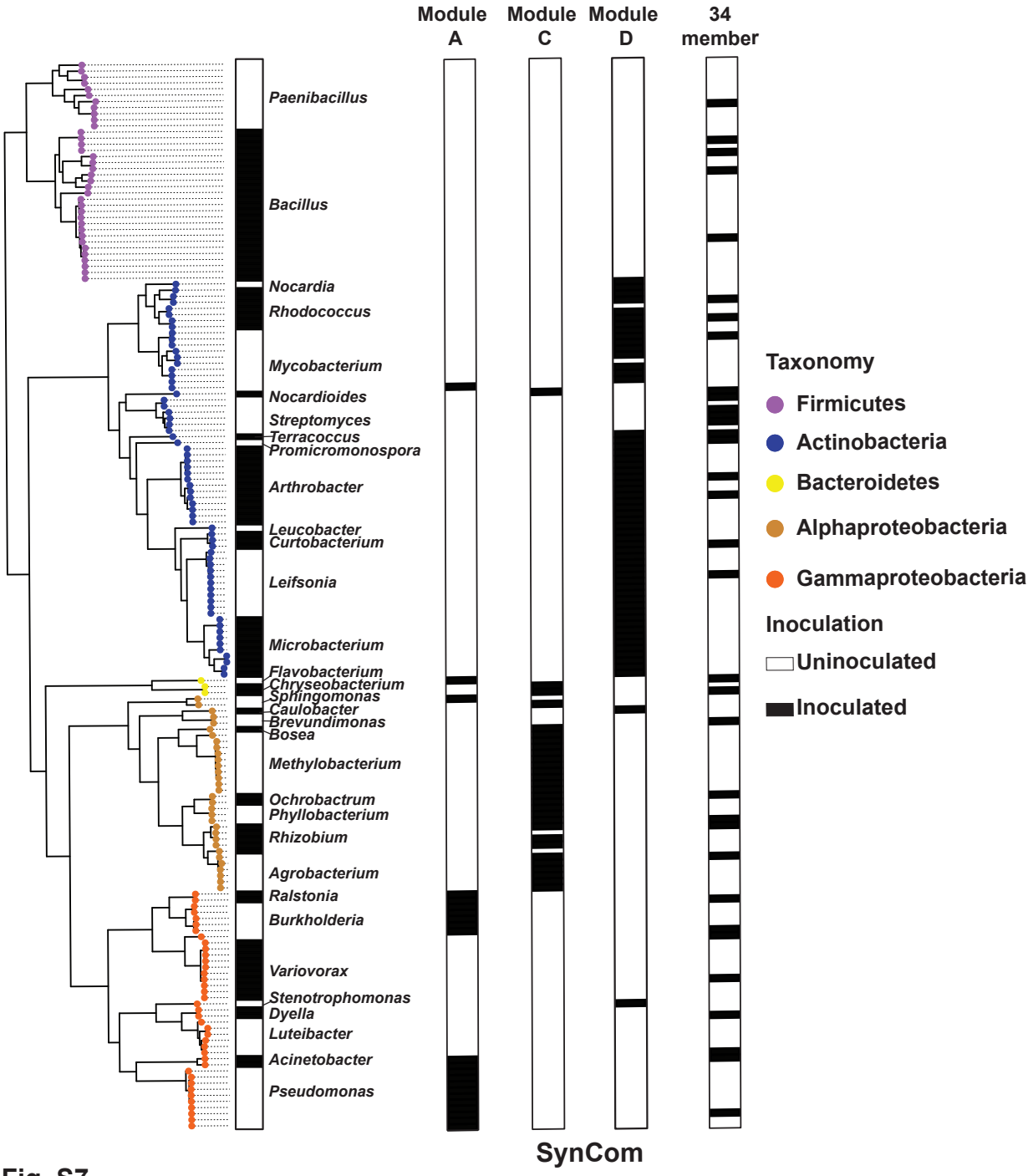

Fig. S7.

Taxonomic composition of the SynCom used in Figure 3D.

Bar graphs showing the isolate composition of SynComs composed by module A (Module A), module C (Module C), module D (Module D) and a 34-member synthetic community (34 member) (2). Isolates are ordered according to the phylogenetic tree on the left side of the panel. The tips of the phylogenetic tree are colored based on the genome-based taxonomy of each isolate. Presence of an isolate across the different SynComs is denoted by a black filled rectangle.

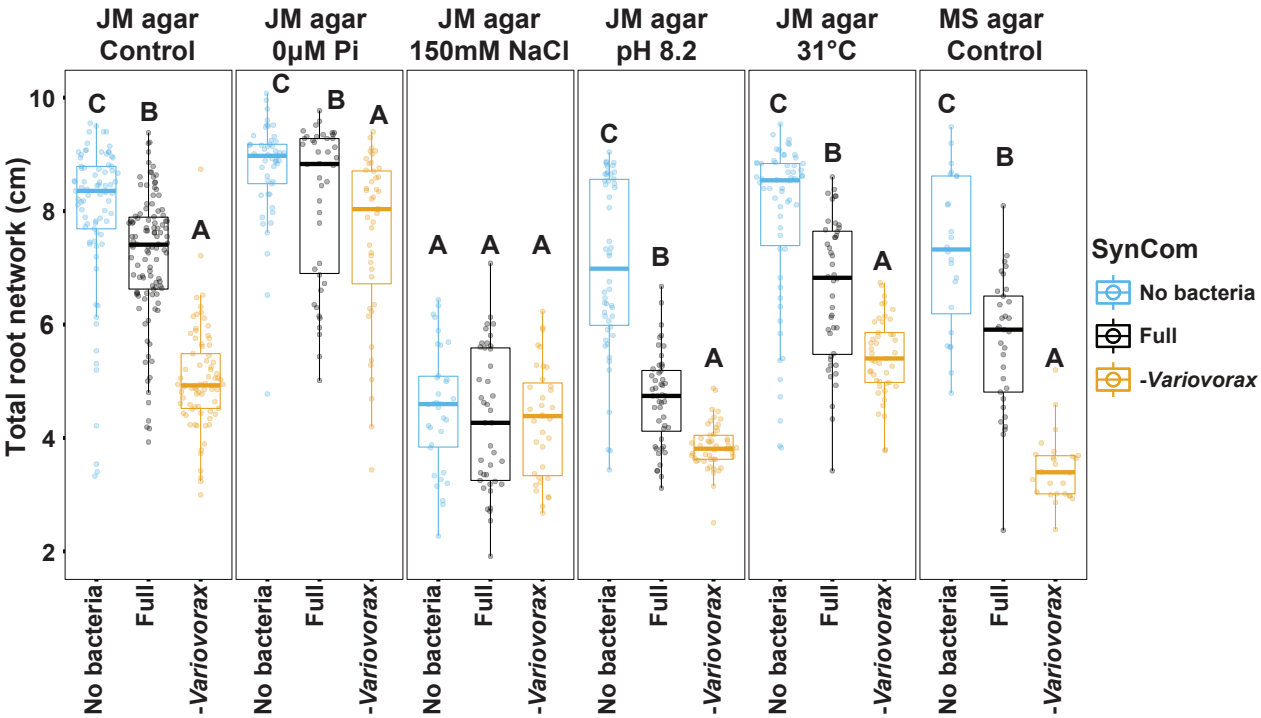

Fig. S8.
***Variovorax* increase total root network length.**
Total root network of seedlings grown axenically (No Bacteria), with the full SynCom (Full) or with the full SynCom excluding *Variovorax* (-*Variovorax)* across different abiotic conditions: full medium (JM agar control), phosphate starvation (JM agar 0 µM Pi), salt stress (JM agar 150 mM NaCl), high pH (JM agar pH 8.2) and high temperature (JM agar 31° C) and media: Johnson medium (JM agar control) and Murashige and Skoog (MS agar control) medium. Letters indicate statistical significance using ANOVA performed within each experimental condition.

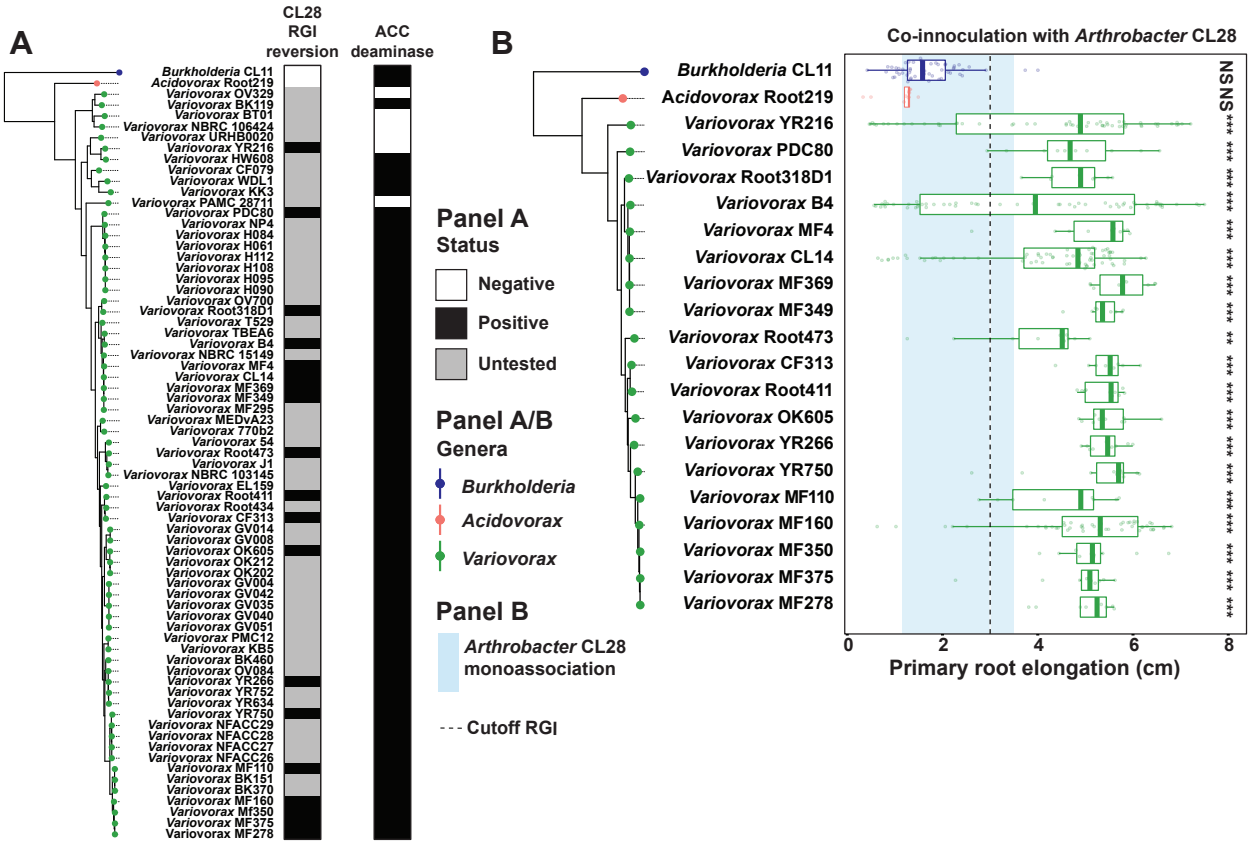

Fig. S9.

Reversion of root growth inhibition is prevalent across the *Variovorax* phylogeny. **(A)** Phylogenetic tree of 54 publicly available *Variovorax* genomes and two outgroup isolates, *Acidovorax* Root219 and *Burkholderia* CL11. The CL28 RGI reversion bar binarizes (positive, negative, untested) the ability of each isolate in the phylogeny to revert the root growth inhibition caused by *Arthrobacter* CL28. The ACC deaminase bar denotes the presence of the KEGG orthology term KO1505 (1-aminocyclopropane-1-carboxylate deaminase) in each of the genomes. **(B)** Phylogenetic tree of 19 *Variovorax* genomes along with two outgroup isolates, *Acidovorax* Root219 and *Burkholderia* CL11 that were tested for their ability to revert the root growth inhibition (RGI) imposed by *Arthrobacter* CL28. The blue vertical strip across the panel denotes the interquartile range of plants treated solely with *Arthrobacter* CL28. The dotted vertical line across the panel denotes the 3 cm cutoff used to classify a treatment as a root growth inhibitor (RGI). Each boxplot is colored according to the genus classification of each isolate. Statistical significance is denoted on the top of each boxplot.

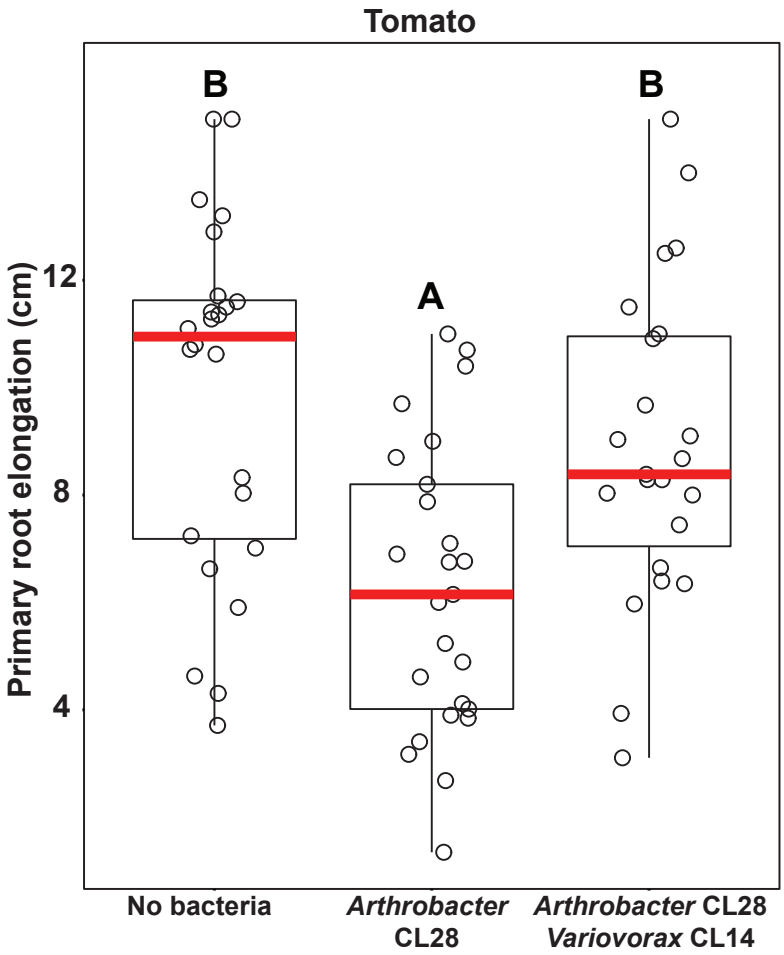

Fig S10.
Reversion of root growth inhibition in tomato seedlings
Primary root elongation of uninoculated seedlings (No bacteria) or seedlings inoculated with the *Arthrobacter* CL28 individually or along with *Variovorax* CL14. Letters indicate post hoc significance.

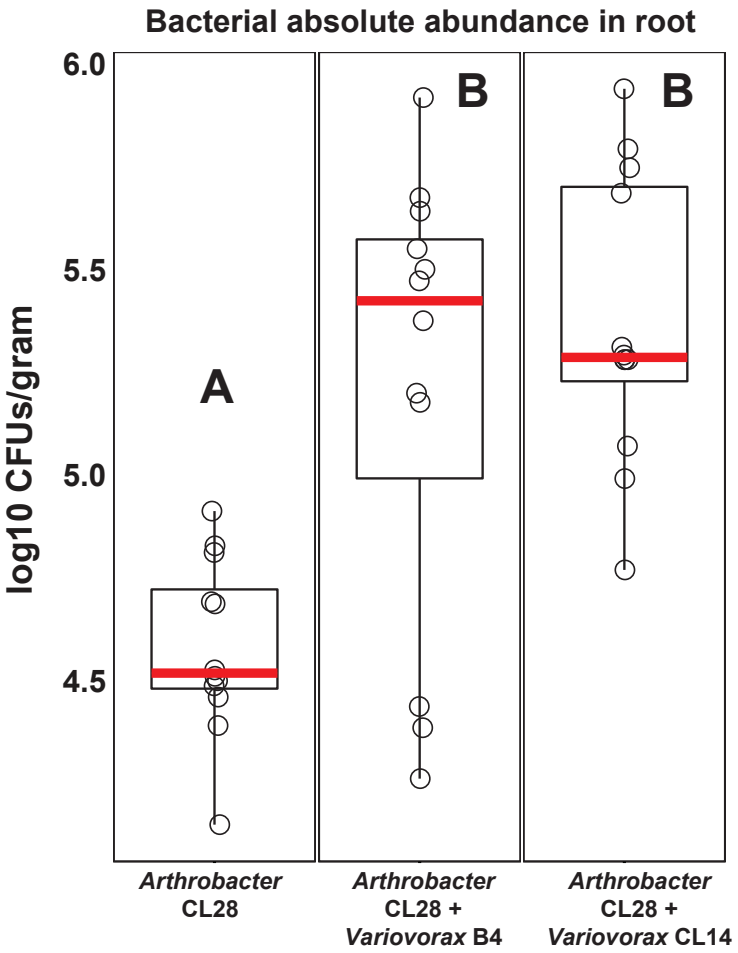

Fig. S11.
***Variovorax* does not inhibit the growth of an RGI strain in Arabidopsis roots.**
In planta colony forming units of *Arthrobacter* CL28 when inoculated alone or with two *Variovorax* representatives: *Variovorax* B4 and *Variovorax* CL14. Log-transformed-Colony forming units (CFU) of *Arthrobacter* CL28 normalized to root weight are shown. To selectively grow *Arthrobacter* CL28, CFUs were counted on Luria Bertani (LB) agar plates containing 50 µg/ml of Apramycin, on which neither *Variovorax* B4 and *Variovorax* CL14 grow.

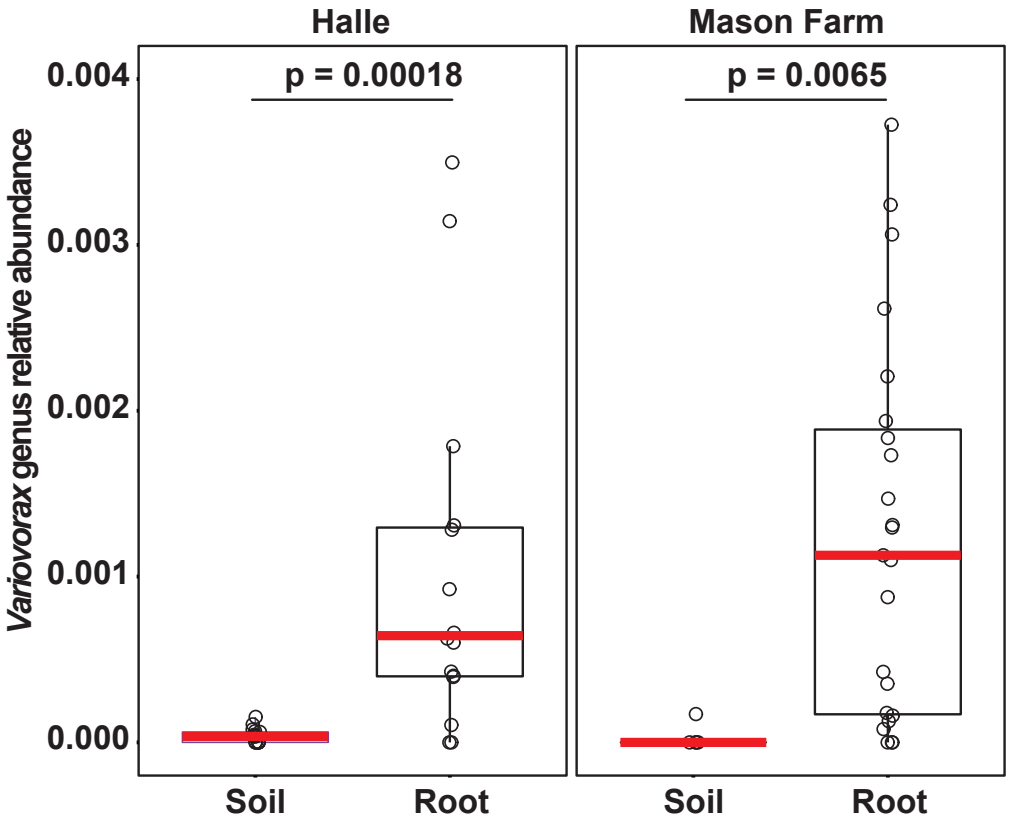

Fig. S12.
***Variovorax* is a root-enriched taxon.**
Cumulative relative abundance of Amplicon Sequence Variants (ASVs) classified as *Variovorax* across the soil and root fractions of *Arabidopsis thaliana* plants sampled across two independent studies (2,25). The cumulative abundance between fractions was compared using Mann-Whitney U test inside each of the two data sets independently.

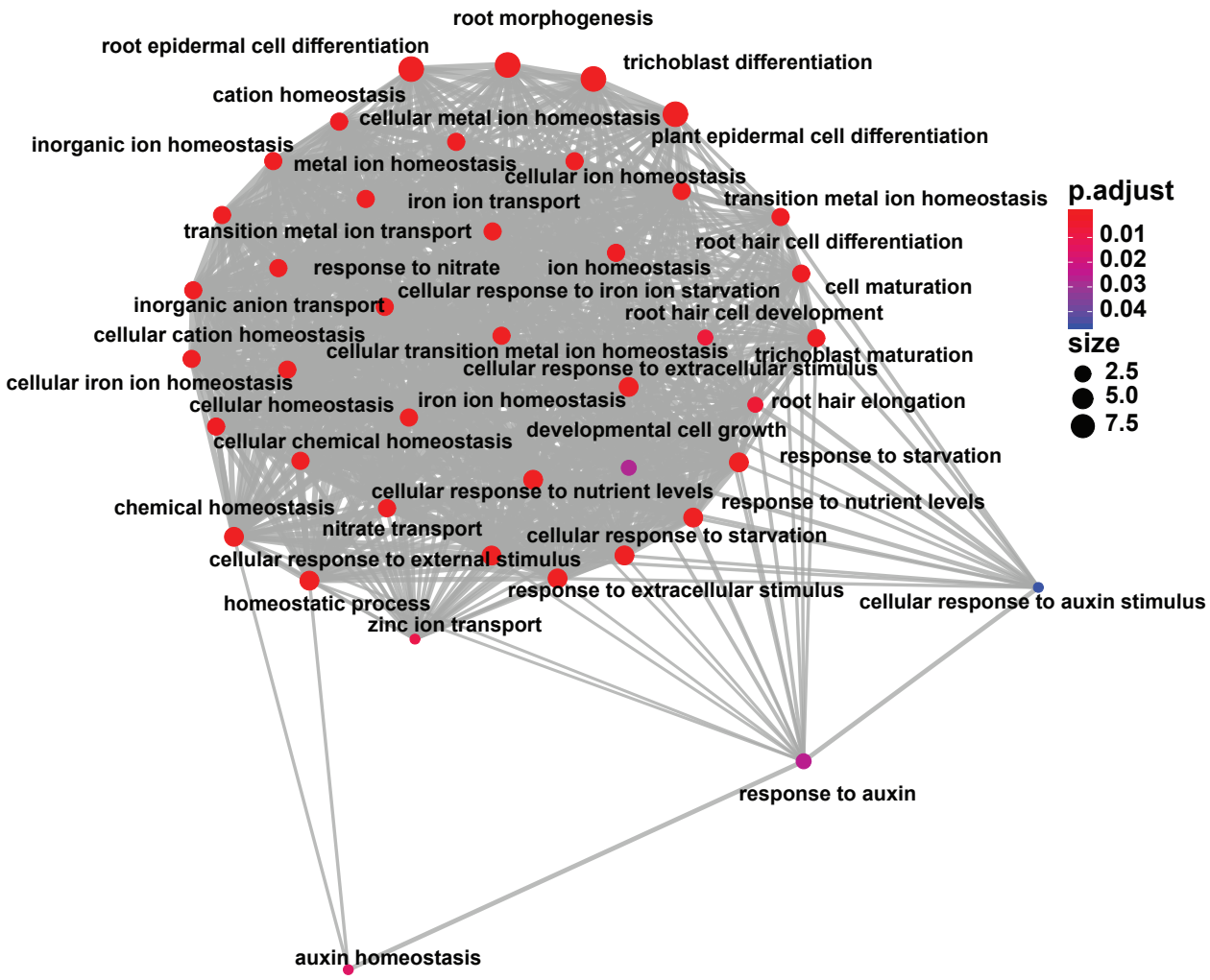

Fig. S13.

Root growth inhibition-related genes are interconnected.

Network of statistically significant gene ontology terms contained in the 18 genes cohesively overexpressed in RGI treatments in the tripartite and dropout systems. See Figure 4A and 4B. The network was computed using the emapplot function from the package clusterProfiler in R. A p-value for terms across the gene ontology was computed using a hypergeometric test, additionally the size of each point (Gene ontology term) denotes the number of genes mapped in that particular term.

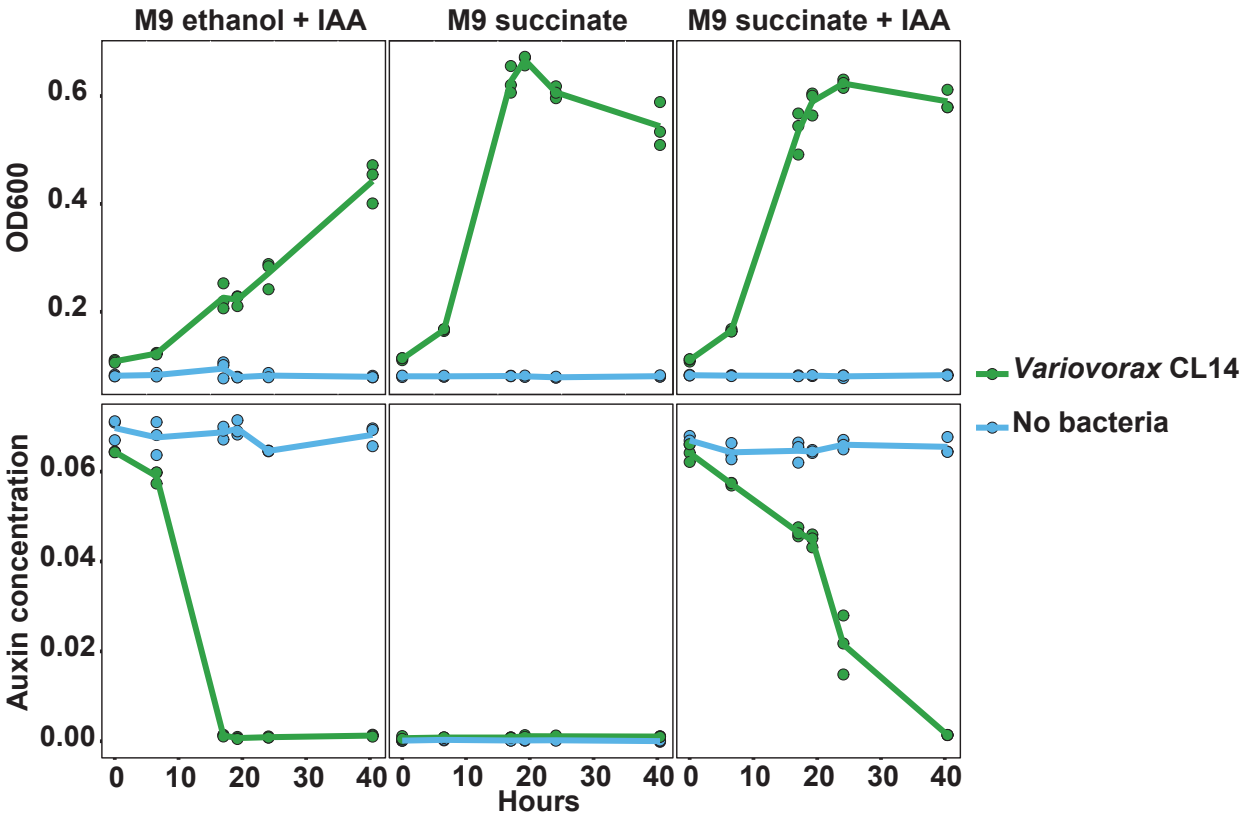

Fig. S14.
***Variovorax* degrades Indole-3-acetic acid.**
Growth curves showing optical density (OD600) (top) and Indole-3-acetic acid (IAA) concentrations (mg/mL) (bottom) in *Variovorax* CL14 cultures grown in M9 media with auxin (left), in M9 media with succinate (center) and M9 media with succinate and auxin (right).

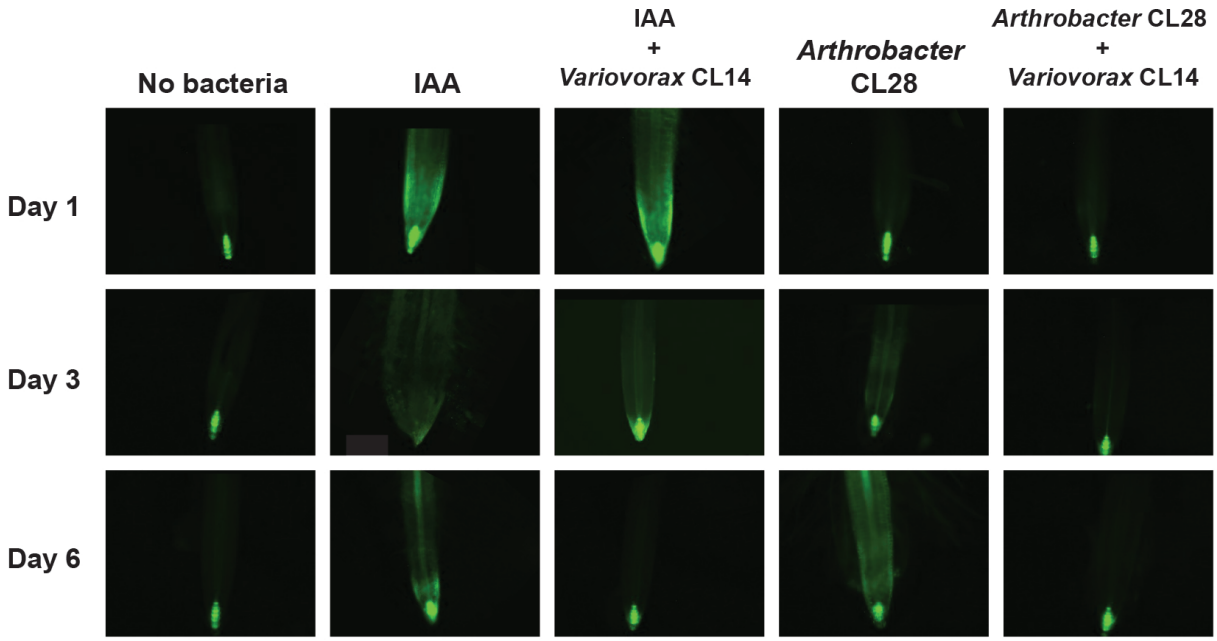

Fig. S15.
***Variovorax* quenches *DR5::GFP* induction.**
Main root tips of plants grown with different Indole-3-acetic acid (IAA) and bacterial treatments. *DR5::GFP* plants were treated with the tripartite system (*Arthrobacter* CL28, *Variovorax* CL14, CL28+CL14), IAA and IAA+*Variovorax* CL14, and GFP fluorescence was imaged 1, 3 and 6 days post inoculation. Fluorescence was quantified in the root elongation zone.

196 **Materials and Methods**

197 **1. Arabidopsis with bacterial SynCom microcosm across four stress gradients (Fig. 1, fig.**
198 **S2-S3, data S2)**

199 a. Bacterial culture and plant-inoculation

200 The 185-member bacterial synthetic community (SynCom) used here contains genome-
201 sequenced isolates obtained from *Brassicaceae* roots, nearly all *Arabidopsis thaliana*, planted in
202 two North Carolina, US, soils. A detailed description of this collection and isolation procedures
203 can be found in (*25*). One week prior to each experiment, bacteria were inoculated from glycerol
204 stocks into 600 µL KB medium in a 96 deep well plate. Bacterial cultures were grown at 28 °C,
205 shaking at 250 rpm. After five days of growth, cultures were inoculated into fresh media and
206 returned to the incubator for an additional 48 hours, resulting in two copies of each culture, 7 days
207 old and 48 hours old. We adopted this procedure to account for variable growth rates of different
208 SynCom members and to ensure that non-stationary cells from each strain were included in the
209 inoculum. After growth, 48-hour and 7-day plates were combined and optical density of cultures
210 was measured at 600 nm (OD_{600}) using an Infinite M200 Pro plate reader (TECAN). All cultures
211 were then pooled while normalizing the volume of each culture to OD_{600}=1. The mixed culture
212 was washed twice with 10 mM $MgCl_2$ to remove spent media and cell debris and vortexed
213 vigorously with sterile glass beads to break up aggregates. OD_{600} of the mixed, washed culture
214 was then measured and normalized to OD_{600}=0.2. 100 µL of this SynCom inoculum was spread
215 on 10 X 10 cm vertical square agar plates with amended Johnson medium (JM; (*2*)) without
216 sucrose prior to transferring seedlings.

217

218 b. In vitro plant growth conditions

219 All seeds were surface-sterilized with 70% bleach, 0.2% Tween-20 for 8 min, and rinsed three
220 times with sterile distilled water to eliminate any seed-borne microbes on the seed surface. Seeds
221 were stratified at 4 °C in the dark for two days. Plants were germinated on vertical square 10 X
222 10 cm agar plates with JM containing 0.5% sucrose, for 7 days. Then, 10 plants were transferred
223 to each of the SynCom-inoculated agar plates. The composition of JM in the agar plates was
224 amended to produce environmental variation. We added to the previously reported phosphate
225 concentration gradient (0, 10, 30, 50, 100, 1000 µm Pi) (*26*) three additional environmental
226 gradients: Salinity (50, 100, 150, 200 mM NaCl), pH (5.5, 7.0, 8.2), Pi concentration and
227 incubation temperature (10, 21, 31˚C). Each gradient was tested separately, in two independent
228 replicas. Each condition included three SynCom+plant samples, two no plant controls and one no
229 bacteria control. Plates were placed in randomized order in growth chambers and grown under a

230 16-h dark/8-h light regime at 21 °C day/18 °C night for 12 days. Upon harvest, DNA was extracted
231 from roots, shoots and agar.
232
233 c. DNA extraction
234 Roots, shoots and agar were harvested separately, pooling 6-8 plants for each sample. Roots
235 and shoots were placed in 2.0 ml Eppendorf tubes with three sterile glass beads. These samples
236 were washed three times with sterile distilled water to remove agar particles and weakly
237 associated microbes. Tubes were stored at -80 ˚C until processing. Root and shoot samples were
238 lyophilized for 48 hours using a Labconco freeze dry system and pulverized using a tissue
239 homogenizer (MPBio). Agar from each plate was stored in 30 ml syringes with a square of
240 sterilized Miracloth (Millipore) at the bottom and kept at -20 °C for one week. Syringes were then
241 thawed at room temperature and samples were squeezed gently through the Miracloth into 50 ml
242 tubes. Samples were centrifuged at max speed for 20 min and most of the supernatant was
243 discarded. The remaining 1-2 ml of supernatant, containing the pellet, was transferred into clean
244 microfuge tubes. Samples were centrifuged again, supernatant was removed, and pellets were
245 stored at -80 °C until DNA extraction. DNA extractions were carried out on ground root and shoot
246 tissue and agar pellets using 96-well-format MoBio PowerSoil Kit (MOBIO Laboratories; Qiagen)
247 following the manufacturer's instruction. Sample position in the DNA extraction plates was
248 randomized, and this randomized distribution was maintained throughout library preparation and
249 sequencing.
250
251 d. Bacterial 16S sequencing
252 We amplified the V3-V4 regions of the bacterial 16S rRNA gene using the primers 338F (5′-ACT
253 CCTACGGGAGGCAGCA-3′) and 806R (5′-GGACTACHVGGGTWTCTAAT-3′). Two barcodes
254 and six frameshifts were added to the 5' end of 338F and six frameshifts were added to the 806R
255 primers, based on the protocol in (*27*). Each PCR reaction was performed in triplicate, and
256 included a unique mixture of three frameshifted primer combinations for each plate. PCR
257 conditions were as follows: 5 µl Kapa Enhancer, 5 µl Kapa Buffer A, 1.25 µl 5 µM 338F, 1.25 µl
258 5 µM 806R, 0.375 µl mixed chloroplast rRNA gene-blocking peptide nucleic acids (PNAs; 1:1 mix
259 of 100 µM plastid PNA and 100 µM mitochondrial PNA (*27*)), 0.5 µl Kapa dNTPs, 0.2 µl Kapa
260 Robust Taq, 8 µl dH2O, 5 µl DNA; temperature cycling: 95°C for 60 s, 24 cycles of 95°C for 15 s,
261 78°C (PNA) for 10 s, 50°C for 30 s, 72°C for 30 s, 4°C until use. Following PCR cleanup, the PCR
262 product was indexed using 96 indexed 806R primers with the same reaction mix as above, and 9
263 cycles of the cycling conditions described in (*2*). PCR products were purified using AMPure XP

264 magnetic beads (Beckman Coulter) and quantified with a Qubit 2.0 fluorometer (Invitrogen).
265 Amplicons were pooled in equal amounts and then diluted to 10 pM for sequencing. Sequencing
266 was performed on an Illumina MiSeq instrument using a 600-cycle V3 chemistry kit. DNA
267 sequence data for this experiment is available at the NCBI bioproject repository (accession
268 PRJNA543313). The abundance matrix, metadata and taxonomy are available at
269 https://github.com/isaisg/variovoraxRGI.
270
271 e. 16S amplicon sequence data processing
272 SynCom sequencing data were processed with MT-Toolbox (*28*). Usable read output from MT-
273 Toolbox (that is, reads with 100% correct primer and primer sequences that successfully merged
274 with their pair) were quality filtered using Sickle (*29*) by not allowing any window with Q-score
275 under 20. The resulting sequences were globally aligned to a reference set of 16S rDNA
276 sequences extracted from genome assemblies of SynCom members. For strains that did not have
277 an intact 16S rDNA sequence in their assembly, we sequenced the 16S rRNA gene using Sanger
278 sequencing. The reference database also included sequences from known bacterial
279 contaminants and Arabidopsis organellar sequences. Sequence alignment was performed with
280 USEARCH v7.1090 (30) with the option 'usearch_global' at a 98% identity threshold. On average,
281 85% of sequences matched an expected isolate. Our 185 isolates could not all be distinguished
282 from each other based on the V3-V4 sequence and were thus classified into 97 unique sequences
283 (USeqs). A USeq encompasses a set of identical (clustered at 100%) V3-V4 sequences coming
284 from a single or multiple isolates.
285
286 Sequence mapping results were used to produce an isolate abundance table. The remaining
287 unmapped sequences were clustered into Operational Taxonomic Units (OTUs) using UPARSE
288 (*31*) implemented with USEARCH v7.1090, at 97% identity. Representative OTU sequences were
289 taxonomically annotated with the RDP classifier (*32*) trained on the Greengenes database (*33*) (4
290 February 2011; Supplementary Data set 1). Matches to Arabidopsis organelles were discarded.
291 The vast majority of the remaining unassigned OTUs belonged to the same families as isolates
292 in the SynCom. We combined the assigned USeq and unassigned OTU count tables into a single
293 count table. In addition to the raw count table, we created rarefied (1000 reads per sample) and
294 relative abundance versions of the abundance matrix for further analyses.
295
296 The resulting abundance tables were processed and analyzed with functions from the ohchibi
297 package (https://github.com/isaisg/ohchibi). An alpha diversity metric (Shannon diversity) was

calculated using the diversity function from the vegan package v2.5-3 (*34*). We used ANOVA to test for differences in alpha diversity between groups. Beta diversity analyses (Principal coordinate analysis, and canonical analysis of principal coordinates) were based on Bray-Curtis dissimilarity calculated from the relative abundance matrices. We used the capscale function from the vegan R package v.2.5-3 (*34*) to compute the canonical analysis of principal coordinates (CAP). To analyze the full dataset (all fraction, all abiotic treatments), we constrained by fraction and abiotic treatment while conditioning for the replica and experiment effect. We explored the abiotic conditions effect inside each of the four abiotic gradients tested (phosphate, salinity, pH and temperature). We performed the Fraction:abiotic interaction analysis within each fraction independently, constraining for the abiotic conditions while conditioning for the replica effect. In addition to CAP, we performed Permutational Multivariate Analysis of Variance (PERMANOVA) using the adonis function from the vegan package v2.5-3 (*34*). We used the package DESeq2 v1.22.1 (*35*) to compute the enrichment profiles for USeqs present in the count table.

We estimated the fraction effect across all the abiotic conditions tested by creating a group variable that merged the fraction variable and the abiotic condition variable together (e.g Root_0Pi, Agar_0Pi). We fitted the following model specification using this group variable:

Abundance ~ Rep + Experiment + group

From the fitted model, we extracted, for all levels within the group variables, the following comparisons: Agar vs Root and Agar vs Shoot. A USeq was considered statistically significant if it had a false discovery rate (FDR) adjusted *p*-value < 0.05.

All scripts and dataset objects necessary to reproduce the synthetic community analyses are deposited in the following github repository: https://github.com/isaisg/variovoraxRGI

f. Co-occurrence analysis

The relative abundance matrix (USeqs X Samples) was standardized across the USeqs by dividing the abundance of each USeq in its sample over the mean abundance of that USeq across all samples. Subsequently, we created a dissimilarity matrix based on the Pearson correlation coefficient between all the pairs of strains in the transformed abundance matrix, using the cor function in the stats base package in R. Finally, hierarchichal clustering (method ward.D2, function hclust) was applied over the dissimilarity matrix constructed above.

g. Heatmap and family enrichment analysis

332 We visualized the results of the GLM model testing the fraction effects across each specific abiotic
333 condition tested using a heatmap. The rows in the heatmap were ordered according to the
334 dendrogram order obtained from the USeqs co-occurrence analysis. The heatmap was colored
335 based on the log2FoldChange output by the GLM model. We highlighted in a black shade the
336 comparisons that were significant (q-value < 0.05). Finally, for each of the four modules we
337 computed for each family present in that module a hypergeometric test testing if that family was
338 overrepresented (enriched) in that particular module. Families whose FDR p-value < 0.1 were
339 visualized in the figure.
340
341 **2. Deconstructing the SynCom to four modules of co-occurring strains (Fig. 2A, 2C and**
342 **data S3).**
343 a. Bacterial culture and plant-inoculation
344 Strains belonging to each module (A, B, C and D, Materials and Methods 1f) were grown in
345 separate deep 96-well plates and mixed as described above (Materials and Methods 1a). The
346 concentration of each module was adjusted to OD=0.05 (1/4 of the concentration of the full
347 SynCom). Each module was spread on the plates either separately, or in combination with
348 another module. In addition, we included a full SynCom control and an uninoculated control,
349 bringing the number of SynCom combinations to 12. We performed the experiment in two
350 independent replicates and each replicate included five plates per SynCom combination.
351
352 b. In vitro plant growth conditions
353 Seed sterilization and germination conditions were the same as Materials and Methods 1b. Plants
354 were transferred to each of the SynCom-inoculated agar plates containing JM without sucrose.
355 Plates were placed in randomized order in growth chambers and grown under a 16-h dark/8-h
356 light regime at 21 °C day/18 °C night for 12 days. Upon harvest, root morphology was measured.
357
358 c. Root and shoot image analysis
359 Plates were imaged twelve days post-transferring, using a document scanner. Primary root length
360 elongation was measured using ImageJ (*36*) and shoot area and total root network were
361 measured with WinRhizo software (Regens Instruments Inc.).
362
363 d. Primary root elongation analyses
364 Primary root elongation was compared across the No Bacteria, full SynCom, single modules and
365 pairs of modules treatments jointly using an ANOVA model controlling for the replicate effect.

366 Differences between treatments were indicated using the confidence letter display (CLD) derived
367 from the Tukey's *post hoc* test implemented in the package emmeans (*37*).
368
369
370 **3. Inoculating plants with all SynCom isolates separately (Fig. 2B, fig. S4 and data S4)**
371 a. Bacterial culture and plant-inoculation.
372 Cultures from each strain in the SynCom were grown in KB medium and washed separately, and
373 $OD_{600}$was adjusted to 0.01 before spreading. We performed the experiment in two independent
374 replicates and each replicate included one plate per each of the 185 strains. In vitro growth
375 conditions were the same as in Materials and Methods 2b. Upon harvest, root morphology was
376 measured (Materials and Methods 2c). Isolates generating an average main root elongation of <3
377 cm were classified as RGI-inducing strains.
378
379 **4. Tripartite plant-microbe-microbe experiments (Fig. 2D-F and data S5-S6)**
380 a. Experimental design
381 To identify strains that revert RGI (Fig. 2D and data S5), we selected all 18 non-RGI inducing
382 strains in module A and co-inoculated them with each of four RGI inducing strains, one from each
383 module. The experiment also included uninoculated controls and controls consisting of each of
384 the 22 strains inoculated alone, amounting to 95 separate bacterial combinations.
385
386 To confirm the ability of *Variovorax* and *Burkholderia* to attenuate RGI induced by diverse bacteria
387 (Fig. 2E and data S6), three RGI attenuating strains were co-inoculated with a selection of 18 RGI
388 inducing strains. The experiment also included uninoculated controls and controls consisting of
389 each of the 21 strains inoculated alone. Thus, the experiment consisted of 76 separate bacterial
390 combinations. We performed each of these two experiments in two independent replicates and
391 each replicate included one plate per each of the strain combinations.
392
393 b. Bacterial culture and plant-inoculation
394 All strains were grown in separate tubes, then washed, and OD_{600} was adjusted to 0.02 before
395 mixing and spreading. In vitro growth conditions were the same as in Materials and Methods 2b.
396 Upon harvest, root morphology was measured (Materials and Methods 2c) and plant RNA was
397 harvested and processed from uninoculated samples, and from samples with *Variovorax* CL14,
398 *Arthrobacter* CL28 and the combination of both (Materials and Methods 4d).
399

400 c. Primary root elongation analysis.
401 We fitted ANOVA models for each RGI-inducing strain tested. Each model compared the primary
402 root elongation with the RGI inducing strains alone against root elongation when the RGI inducing
403 strain was co-inoculated with other isolates. The *p*-values for all the comparisons were corrected
404 for multiple testing using false discovery rate.
405
406 d. RNA extraction
407 RNA was extracted from *A. thaliana* seedlings following (*38*). Four seedlings were harvested from
408 each sample and samples were flash frozen and stored at -80 ˚C until processing. Frozen
409 seedlings were ground in liquid nitrogen, then homogenized in a buffer containing 400 µl of Z6-
410 buffer; 8 M guanidine HCl, 20 mM MES, 20 mM EDTA at pH 7.0. 400 µL
411 phenol:chloroform:isoamylalcohol, 25:24:1 was added, and samples were vortexed and
412 centrifuged (20,000 g, 10 minutes) for phase separation. The aqueous phase was transferred to
413 a new 1.5 ml tube and 0.05 volumes of 1 N acetic acid and 0.7 volumes 96% ethanol were added.
414 The RNA was precipitated at -20 °C overnight. Following centrifugation (20,000 g, 10 minutes,
415 4°C), the pellet was washed with 200 µl sodium acetate (pH 5.2) and 70% ethanol. The RNA was
416 dried and dissolved in 30 µL of ultrapure water and stored at -80 °C until use.
417
418 e. Plant RNA sequencing
419 Illumina-based mRNA-Seq libraries were prepared from 1 µg RNA following (*4*). mRNA was
420 purified from total RNA using Sera-mag oligo(dT) magnetic beads (GE Healthcare Life Sciences)
421 and then fragmented in the presence of divalent cations (Mg^{2+}) at 94°C for 6 minutes. The
422 resulting fragmented mRNA was used for first-strand cDNA synthesis using random hexamers
423 and reverse transcriptase, followed by second-strand cDNA synthesis using DNA Polymerase I
424 and RNAseH. Double-stranded cDNA was end-repaired using T4 DNA polymerase, T4
425 polynucleotide kinase, and Klenow polymerase. The DNA fragments were then adenylated using
426 Klenow exo-polymerase to allow the ligation of Illumina Truseq HT adapters (D501–D508 and
427 D701–D712). All enzymes were purchased from Enzymatics. Following library preparation,
428 quality control and quantification were performed using a 2100 Bioanalyzer instrument (Agilent)
429 and the Quant-iT PicoGreen dsDNA Reagent (Invitrogen), respectively. Libraries were sequenced
430 using Illumina HiSeq4000 sequencers to generate 50-bp single-end reads.
431
432 f. RNA-Seq read processing
433 Initial quality assessment of the Illumina RNA-Seq reads was performed using FastQC v0.11.7

434 (*39*). Trimmomatic v0.36 (*40*) was used to identify and discard reads containing the Illumina
435 adaptor sequence. The resulting high-quality reads were then mapped against the TAIR10
436 Arabidopsis reference genome using HISAT2 v2.1.0 (*41*) with default parameters. The
437 featureCounts function from the Subread package (*42*) was then used to count reads that mapped
438 to each one of the 27,206 nuclear protein-coding genes. Evaluation of the results of each step of
439 the analysis was performed using MultiQC v1.1 (*43*). Raw sequencing data and read counts are
440 available at the NCBI Gene Expression Omnibus accession number GSE131158.
441
442 **5. *Variovorax* drop-out experiment (Fig. 3A-C and data S7)**
443 a. Bacterial culture and plant-inoculation.
444 The entire SynCom, excluding all 10 *Variovorax* isolates and all five *Burkholderia* isolates was
445 grown and prepared as described above (Materials and Methods 1a). The *Variovorax* and
446 *Burkholderia* isolates were grown in separate tubes, washed and added to the rest of the SynCom
447 to a final OD_{600} of 0.001 (the calculated OD_{600} of each individual strain in a 185-Member SynCom
448 at a total of OD_{600} of 0.2), to form the following five mixtures: (i) Full community – all *Variovorax*
449 and *Burkholderia* isolates added to the SynCom; (ii) *Burkholderia* drop-out – only *Variovorax*
450 isolates added to the SynCom; (iii) *Variovorax* drop-out – only *Burkholderia* isolates added to the
451 SynCom; (iv) *Variovorax* and *Burkholderia* drop-out – no isolates added to the SynCom; (v)
452 Uninoculated plants – no SynCom. The experiment consisted of six plates per SynCom mixture,
453 amounting to 30 plates. Upon harvest, root morphology was measured and analyzed (Materials
454 and Methods 1c,4c); and Bacterial DNA (Materials and Methods 1d) and plant RNA (Materials
455 and Methods 4d-e) were harvested and processed.
456
457 **6. *Variovorax* drop-out under varying abiotic contexts (Fig. 3E and data S7)**
458 a. Bacterial culture and plant-inoculation.
459 The composition of JM in the agar plates was amended to produce abiotic environmental
460 variation. These amendments included salt stress (150 mM NaCl), low Phosphate (10 µm
461 Phosphate), high pH (pH 8.2) and high temperature (plates incubated at 31 ˚C), as well as an un-
462 amended JM control. Additionally, we tested a different media (1/2-strength Murashige and Skoog
463 [MS]) and a soil-like substrate. As a soil-like substrate, we used calcined clay (Diamond Pro),
464 prepared as follows: 100 ml of clay was placed in Magenta GA7 vessels. The vessels were then
465 autoclaved twice. 40 ml of liquid JM was added to the vessels, with the corresponding bacterial
466 mixture spiked into the media at a final OD_{600} of 5E-4. Four 1-week old seedlings were transferred

467 to each vessel, and vessels were covered with Breath-Easy gas permeable sealing membrane
468 (Research Products International) to maintain sterility and gas exchange.
469
470 The entire SynCom, excluding all 10 *Variovorax* isolates was grown and prepared as described
471 above (Materials and Methods 1a). The *Variovorax* isolates were grown in separate tubes,
472 washed and added to the rest of the SynCom to a final OD_{600} of 0.001 (the calculated OD_{600} of
473 each individual strain in a 185-Member SynCom at an OD_{600} of 0.2), to form the following five
474 mixtures: (i) Full community – all *Variovorax* isolates added to the SynCom; (ii) *Variovorax* drop-
475 out – no isolates added to the SynCom; (iii) Uninoculated plants – no SynCom.
476
477 We inoculated all three SynCom combinations in all seven abiotic treatments, amounting to 21
478 experimental conditions. We performed the experiment in two independent replicates and each
479 replicate included three plates per experimental conditions, amounting to 63 plates per replicate.
480 Upon harvest, root morphology was measured (Materials and Methods 2c); and Bacterial DNA
481 (Materials and Methods 1c-e) and plant RNA (Materials and Methods 4d-f) were harvested and
482 processed, excluding the clay treatment.
483
484 b. Root image analysis
485 For agar plates, roots were imaged as described above (Materials and Methods 2c). For calcined
486 clay pots, four weeks post-transferring, pots were inverted, and whole root systems were gently
487 separated from the clay by washing with water. Root systems were spread over an empty petri
488 dish and scanned using a document scanner.
489
490 c. Primary root elongation and total root network analysis.
491 Primary root elongation was compared between SynCom treatments within each of the different
492 abiotic contexts tested independently. Differences between treatments were indicated using the
493 confidence letter display (CLD) derived from the Tukey's *post hoc* test implemented in the
494 package emmeans.
495
496 d. Bacterial 16S data analysis
497 To be able to compare shifts in the community composition of samples treated with and without
498 the *Variovorax* genus, we *in silico* removed the 10 *Variovorax* isolates from the count table of
499 samples inoculated with the Full community treatment. We then merged this count table with the
500 count table constructed from samples inoculated without the *Variovorax* genus (*Variovorax* drop-

501 out treatment). Then, we calculated a relative abundance of each USeq across all the samples
502 using the merged count matrix. Finally, we applied Canonical Analysis of Principal Coordinates
503 (CAP) over the merged relative abundance matrix to control for the replica effect. In addition, we
504 utilized the function adonis from the vegan R package to compute a PERMANOVA test over the
505 merged relative abundance matrix and we fitted a model evaluating the fraction and SynCom
506 (presence of *Variovorax*) effects over the assembly of the community.
507
508 **7. *Variovorax* drop-out under varying biotic contexts (Fig. 3D, fig S7 and data S7)**
509 a. Bacterial culture and plant-inoculation.
510 Strains belonging to modules A (excluding *Variovorax*), C and D were grown in separate wells in
511 deep 96-well plates and mixed as described above (Materials and Methods 1a). The
512 concentration of each module was adjusted to OD=0.05 (1/4 of the concentration of the full
513 SynCom). The *Variovorax* isolates were grown in separate tubes, washed and added to the rest
514 of the SynCom to a final OD_{600} of 0.001.
515
516 In a separate experiment, the 35-member SynCom used in (*2*) was grown, excluding *Variovorax*
517 CL14, to create a taxonomically diverse, *Variovorax*-free subset of the full 185 community. The
518 concentration of this SynCom was adjusted to OD_{600}=0.05. The *Variovorax* isolates were grown
519 in separate tubes, washed and added to the rest of the SynCom to a final OD_{600} of 0.001.
520
521 These two experiments included the following mixtures (fig S7 and data S7): (i) Module A
522 excluding *Variovorax*; (ii) Module C; (iii) Module D; (iv) Module A including *Variovorax*; (v) Module
523 C + all 10 *Variovorax*; (vi) Module D + all 10 *Variovorax*; (vii) 35-member SynCom excluding
524 *Variovorax*; (viii) 34-member SynCom + all 10 *Variovorax*; (ix) uninoculated control. The
525 experiment with modules A, C and D was performed in two independent experiments, with two
526 plates per treatment in each. The experiment with the 34-member SynCom was performed once,
527 with 5 plates per treatment. Upon harvest, root morphology was measured (Materials and
528 Methods 2c).
529
530 b. Primary root elongation analysis.
531 We directly compared differences between the full SynCom and *Variovorax* drop-out treatment
532 using a *t*-test and adjusting the *p*-values for multiple testing using false discovery rate.
533
534 **8. Phylogenetic inference of the SynCom and *Variovorax* Isolates (Fig 2A, fig. S1A, S4, S7**

535 **and S9A-B)**

536 To build the phylogenetic tree of the SynCom isolates, we used the super matrix approach
537 previously described in (*25*). We scanned 120 previously defined marker genes across the 185
538 isolate genomes from the SynCom utilizing the hmmsearch tool from the hmmer v3.1b2 (*44*).
539 Then, we selected 47 markers that were present as single copy genes in 100% of our isolates.
540 Next, we aligned each individual marker using MAFFT (*45*) and filtered low quality columns in the
541 alignment using trimAl (*46*). Then, we concatenated all filtered alignments into a super alignment.
542 Finally, FastTree v2.1 (*47*) was used to infer the phylogeny utilizing the WAG model of evolution.
543 For the *Variovorax* relative's tree, we chose 56 markers present as single copy across 124
544 Burkholderiales isolates and implemented the same methodology described above.

545

546 **9. Measuring how prevalent is the RGI attenuation trait across the *Variovorax* phylogeny**
547 **(fig. S9A-B, data S1 and data S8)**

548 a. Bacterial culture and plant-inoculation.

549 Fifteen *Variovorax* strains from across the genus' phylogeny were each co-inoculated with the
550 RGI inducer *Arthrobacter* CL28. All 16 strains were grown in separate tubes, then washed, and
551 $OD_{600}$was adjusted to 0.01 before mixing. Pairs of strains were mixed in 1:1 ratios and spread
552 onto agar prior to seedling transfer. The experiment also included uninoculated controls and
553 controls consisting of each of the 16 strains inoculated alone. Thus, the experiment consisted of
554 32 separate bacterial combinations. We performed the experiment one time, which included 3
555 plates per bacterial combination. Upon harvest, root morphology was measured (Materials and
556 Methods 2c). Primary root elongation was analyzed as described above (Materials and Methods
557 4c).

558

559 **10. Measuring root growth inhibition in tomato seedlings (fig. S10 and data S9)**

560 a. Experimental design

561 This experiment included the following treatments: (i) No bacteria, (ii) *Arthrobacter* CL28, (iii)
562 *Variovorax* CL14 and (iv) *Arthrobacter* CL28 + *Variovorax* CL14. Each treatment was repeated in
563 three separate agar plates with five tomato seedlings per plate. The experiment was repeated in
564 two independent replicates.

565

566 b. Bacterial culture and plant-inoculation

567 All strains were grown in separate tubes, then washed, and OD_{600} was adjusted to 0.01 before
568 mixing and spreading. 400 µL of each bacterial treatment was spread on 20 X 20 agar plates
569 containing JM agar with no sucrose.
570
571 c. In vitro plant growth conditions
572 We used Heinz 1706 seeds. All seeds were soaked in sterile distilled water for 15 min, then
573 surface-sterilized with 70% bleach, 0.2% Tween-20 for 15 min, and rinsed five times with sterile
574 distilled water to eliminate any seed-borne microbes on the seed surface. Seeds were stratified
575 at 4 °C in the dark for two days. Plants were germinated on vertical square 10 X 10 cm agar plates
576 with JM containing 0.5% sucrose, for 7 days. Then, 5 plants were transferred to each of the
577 SynCom-inoculated agar plates. Upon harvest, root morphology was measured. (Materials and
578 Methods 2c).
579
580 c. Primary root elongation analysis.
581 Differences between treatments were indicated using the confidence letter display (CLD) derived
582 from the Tukey's *post hoc* test from an ANOVA model.
583
584
585 **11. Enumeration of *Arthrobacter* CL28 colony forming units from roots (fig. S11 and data**
586 **S10)**
587 Arabidopsis seedlings were inoculated with (i) *Arthrobacter* CL28 alone, (ii) *Arthrobacter* CL28 +
588 *Variovorax* CL14 or (iii) *Arthrobacter* CL28 + *Variovorax* B4, as described above (Material and
589 Methods 4b). Each bacterial treatment included four separate plates, with nine seedlings in each
590 plate. Upon harvest, all seedlings were placed in pre-weighed 2.0 ml Eppendorf tubes containing
591 three glass beads, three seedlings per tube (producing 12 data points per treatment). Roots were
592 weighed, then crushed using a bead beater. The resulting suspension was plated on Luria Bertani
593 agar plates containing 50 µg/ml of Apramycin, in a dilution series, and colonies were counting
594 after incubation of 48 hours at 28˚ C.
595
596
597 **12. RNA-Seq analysis (Fig. 4A-C, fig. S13 and data S11-12)**
598 a. Detection of RGI-induced genes (Fig. 4A-B)
599 To measure the transcriptional response of the plant to the different SynCom combinations, we
600 used the R package DESeq2 v.1.22.1 (*35*). The raw count genes matrixes for the dropout and

601 tripartite experiments were used independently to define differentially expressed genes (DEGs).
602 For the analysis of both experiments we fitted the following model specification:
603 Abundance Gene ~ SynCom
604 From the fitted models we derived the following contrasts to obtain differentially expressed genes
605 (DEGs). A gene was considered differentially expressed if it had a *q*-value < 0.1. For the tripartite
606 system (Materials and Methods 4), we performed the following contrasts: *Arthrobacter* CL28 vs
607 No Bacteria (NB) and *Arthrobacter* CL28 vs *Arthrobacter* CL28 co-inoculated with *Variovorax*
608 CL14. The logic behind these two contrasts was to identify genes that were induced in RGI plants
609 (*Arthrobacter* CL28 vs NB) AND repressed by *Variovorax* CL14. For the dropout system
610 (Materials and Methods 5), we performed the following contrasts, *Variovorax* drop-out vs NB, and
611 *Variovorax* drop-out vs full SynCom. The logic behind these two contrasts was identical to the
612 tripartite system: to identify genes that are associated with the RGI phenotype (*Variovorax* drop-
613 out vs NB contrast) AND repressed when *Variovorax* are present (*Variovorax* drop-out vs full
614 SynCom contrast).
615
616 For visualization purposes, we applied a variance stabilizing transformation to the raw count gene
617 matrix. We then standardized each gene expression (z-score) along the samples. We subset
618 DEGs from this standardized matrix and calculated the mean z-score expression value for each
619 SynCom treatment.
620
621 To identify the tissue specific expression profile of the 18 intersecting genes between the tripartite
622 and dropout systems, we downloaded the spatial expression profile of each gene from the
623 Klepikova atlas (*14*) using the Bio-analytic resource of plant biology platform. Then, we
624 constructed a spatial expression matrix of the 18 genes and computed pairwise Pearson
625 correlation between all pairs of genes. Finally, we applied hierarchical clustering to this correlation
626 matrix.
627
628 b. Comparison with acute auxin response dataset (Figure 4C)
629 We applied a variance stabilizing transformation to the raw count gene matrix. We then
630 standardized each gene expression (z-score) along the samples. From this matrix, we subset 12
631 genes that in a previous study (*15*) exhibited the highest fold change between auxin treated and
632 untreated samples. Finally, we calculated the mean z-score expression value of each of these 12
633 genes across the SynCom treatments. We estimated the statistical significance of the trend of
634 these 12 genes between a pair of SynCom treatments (Full SynCom vs *Variovorax* drop-out,

635 *Arthrobacter* CL28 vs *Arthrobacter* CL28 plus *Variovorax* CL14) using a permutation approach:
636 we estimated a *p*-value by randomly selecting 12 genes 10000 times from the expression matrix
637 and comparing the mean expression between the two SynCom treatments (e.g Full SynCom vs
638 *Variovorax* drop-out) with the actual mean expression value from the 12 genes reported as robust
639 auxin markers.
640
641 **13. Measuring the ability of *Variovorax* to attenuate RGI induced by small molecules**
642 **(Figure 4D and data S13)**
643 a. Bacterial culture and plant-inoculation.
644 We embedded each of the following compounds in JM plates: 100 nM IAA, 1μM IAA, 100 nM
645 ACC, 100 nM 2,4-d, 100 nM flg22, 100 nM BAP and 100 nM Zeatin. Plates with each compound
646 were inoculate with one of the *Variovorax* strains CL14, MF160, B4 or YR216 or with *Burkholderia*
647 CL11. These strains were grown in separate tubes, then washed, and OD_{600} was adjusted to 0.01
648 before spreading 100μL on plates. In addition, we included uninoculated controls for each
649 compound. We also included unamended JM plates inoculated with the RGI inducer *Arthrobacter*
650 CL28 co-inoculated with each of the *Variovorax/Burkholderia* strains or alone. Thus, the
651 experiment included 42 individual treatments. The experiment was repeated twice, with three
652 independent replicates per experiment. Upon harvest, root morphology was measured (Materials
653 and Methods 2c).
654
655 b. Primary root elongation analysis.
656 Primary root elongation was compared between bacterial treatments within each of root growth
657 inhibition treatments tested. Differences between treatments were estimated as described above
658 (Materials and Methods 4c). We plotted the estimated means with 95% CI of each bacterial
659 treatment across the different RGI treatments.
660
661
662 **14. In vitro growth of *Variovorax* (fig. S14)**
663 *Variovorax* CL14 was grown in 5mL cultures for 40 hours at 28 ˚C in 1x M9 minimal salts media
664 (Sigma M6030) supplemented with 2mM $MgSO_4$, 0.1mM $CaCl_2$, 10μM $FeSO_4$, and a carbon
665 source: either 15mM succinate alone, 0.4mM Indole-3-acetic acid (IAA) with 0.5% Ethanol from
666 IAA solubilization, or both. Optical density at 600 nm and IAA concentrations were measured at
667 six time points. IAA concentrations were measured using the Salkowski method modified from
668 (*48*). 100uL of Salkowski reagent (10mM $FeCl_3$ in 35% perchloric acid) was mixed with 50uL

669 culture supernatant or IAA standards and color was allowed to develop for 30 min prior to
670 measuring the absorbance at 530nm.
671
672 **15. Measuring plant Auxin response *in-vivo* using a bioreporter line (Fig. 4E-F and data**
673 **S14)**
674 a. Bacterial culture and plant-inoculation.
675 7-day old transgenic Arabidopsis seedlings expressing the *DR5::GFP* reporter construct (*49*) were
676 transferred onto plates containing: (i) 100 nM IAA, (ii) *Arthrobacter* CL28, (iii) 100 IAA + *Variovorax*
677 CL14, (iv) *Arthrobacter* CL28 + *Variovorax* CL14, (v) the *Variovorax* drop-out SynCom, (vi) the
678 full SynCom, (vii) uninoculated plates. For treatments ii,iii, Bacterial strains were grown in
679 separate tubes, then washed, and OD_{600} was adjusted to 0.01. For treatment iv, OD-adjusted
680 cultures were mixed in 1:1 ratios and spread onto agar prior to seedling transfer. Cultures for
681 treatments v and vi were prepared as described above (Materials and Methods 6a).
682 b. Fluorescence microscopy.
683 GFP fluorescence in the root elongation zone of 8-10 plants per treatment were visualized using
684 a Nikon Eclipse 80i fluorescence microscope at days 1, 3, 6, 9 and 13 post inoculation. The
685 experiment was performed in two independent replicates.
686 From each root imaged, 10 random 30 X 30 pixel squares were sampled and average GFP
687 intensity was measured using imageJ (*36*). Treatments were compared within each time point
688 using ANOVA tests with Tukey's post hoc in the R base package emmeans. For visualization
689 purposes we plotted the estimated means of each bacterial across the different timepoints.
690
691 **16. Measuring the dual role of auxin and ethylene perception in SynCom-induced RGI (Fig.**
692 **4F and data S15)**
693 a. Bacterial culture and plant-inoculation.
694 We transferred four 7-day old wild type seedling and four *axr1-2* seedlings to each plate in this
695 experiment. The plates contained one of five bacterial treatments: (i) *Arthrobacter* CL28, (ii)
696 *Arthrobacter* CL28 + *Variovorax* CL14, (iii) *Variovorax* drop-out SynCom, (iv) Full SynCom, (v)
697 uninoculated, prepared as described above (Materials and Methods 15a) Plates were placed
698 vertically inside sealed 86 X 68 cm Ziploc bags. In one of the bags, we placed an open water
699 container with 80 2.5 gram sachets containing 0.014% 1-MCP (Ethylene Buster, Chrystal
700 International BV). In the second bag we added, as a control, an open water container. Both bags
701 were placed in the growth chamber for 12 days. After 6 days of growth, we added 32 additional

702 sachets to the 1-MCP-treated bag to maintain 1-MCP concentrations in the air. Upon harvest, root
703 morphology was measured (Materials and Methods 2c).
704
705 b. Primary root elongation analysis.
706 Primary root elongation was standardized to the No bacteria control of each genotype, and
707 compared between genotype/1-MCP treatments within the *Arthrobacter* CL28 treatment and the
708 *Variovorax* drop-out SynCom treatment, independently. Differences between treatments were
709 estimated as described above (Materials and Methods 4c). We plotted the estimated means with
710 95% CI of each bacterial treatment across the four genotypes. We calculated the interquartile
711 range for the Full and *Arthrobacter* CL28/*Variovorax* CL14 treatments pooling the four
712 genotypes/treatments.
713
714
715 **17. Preparation of binerized plant images (Fig 2C, 3B and fig. S5-S6)**
716 To present representative root images, we increased contrast and subtracted background in
717 imageJ, then cropped the image to select representative roots. Neighboring roots were manually
718 erased from the cropped image.
719
720 **18. Mining *Variovorax* genomes for auxin degradation operons and ACC-deminase genes**
721 **(Discussion).**
722 We used local alignment (BLASTp) to search for the presence of the10 genes (*iacA*, *iacB*, *iacC*,
723 *iacD*, *iacE*, *iacF*, *iacG*, *iacH*, *iacI*, and *iacY*) of a previously characterized auxin degradation
724 operon (*50*) across the 10 *Variovorax* isolates in our bacterial synthetic community and searched
725 for hotspots of clustered hits within genomes (<10kb between genes). Across the 10 *Variovorax*
726 isolates scanned, we could not reconstruct any hotspot that recapitulated the previously described
727 operon. Additionally to the *iac* operon, we scanned the auxin degradation operon described in
728 (*51*) and could not identify it across the *Variovorax* isolates. Another piece of evidence that
729 supports the fact that *Variovorax* lack these degradation operons was the weak (< 30%) identity
730 between the spurious hits we did find to some of the components of these operons across the
731 *Variovorax* genomes.
732 We searched for the ACC deaminase gene by looking for the KEGG orthology id K01505 (1-
733 aminocyclopropane-1-carboxylate deaminase) across our genomes.
734

735 **References and Notes:**

736 1. K. Hiruma *et al.*, Root Endophyte Colletotrichum tofieldiae Confers Plant Fitness Benefits
737 that Are Phosphate Status Dependent. *Cell*. **165**, 464–474 (2016).

738 2. G. Castrillo *et al.*, Root microbiota drive direct integration of phosphate stress and
739 immunity. *Nature*. **543** (2017), doi:10.1038/nature21417.

740 3. P. Durán *et al.*, Microbial Interkingdom Interactions in Roots Promote Arabidopsis Survival.
741 *Cell*. **175**, 973–983.e14 (2018).

742 4. S. Herrera Paredes *et al.*, Design of synthetic bacterial communities for predictable plant
743 phenotypes. *PLOS Biol.* **16**, e2003962 (2018).

744 5. A. C. Huang *et al*., A specialized metabolic network selectively modulates Arabidopsis root
745 microbiota. *Science* **364**, eaau6389 (2019).

746 6. S. A. Hogenhout, R. A. L. Van der Hoorn, R. Terauchi, S. Kamoun, Emerging Concepts in
747 Effector Biology of Plant-Associated Organisms. *Mol. Plant-Microbe Interact.* **22**, 115–122
748 (2009).

749 7. D. Faure, D. Vereecke, J. H. J. Leveau, Molecular communication in the rhizosphere. *Plant*
750 *Soil*. **321**, 279–303 (2009).

751 8. P. Mylona, K. Pawlowski, T. Bisseling, Symbiotic Nitrogen Fixation. *Plant Cell*. **7**, 869–885
752 (1995).

753 9. Y. Helman, L. Chernin, Silencing the mob: disrupting quorum sensing as a means to fight
754 plant disease. *Mol. Plant Pathol.* **16**, 316–329 (2015).

755 10. J. H. J. Leveau, S. E. Lindow, Utilization of the plant hormone indole-3-acetic acid for
756 growth by Pseudomonas putida strain 1290. *Appl. Environ. Microbiol.* **71**, 2365–71 (2005).

757 11. A. Zúñiga *et al.*, Quorum Sensing and Indole-3-Acetic Acid Degradation Play a Role in
758 Colonization and Plant Growth Promotion of *Arabidopsis thaliana* by *Burkholderia*
759 *phytofirmans* PsJN. *Mol. Plant-Microbe Interact.* **26**, 546–553 (2013).

760 12. J. R. Leadbetter, E. P. Greenberg, Metabolism of acyl-homoserine lactone quorum-sensing
761 signals by Variovorax paradoxus. *J. Bacteriol.* **182**, 6921–6 (2000).

762 13. C. R. Fitzpatrick *et al.*, Assembly and ecological function of the root microbiome across
763 angiosperm plant species. *Proc. Natl. Acad. Sci. U. S. A.* **115**, E1157–E1165 (2018).

764 14. A. V. Klepikova, A. S. Kasianov, E. S. Gerasimov, M. D. Logacheva, A. A. Penin, A high
765 resolution map of the *Arabidopsis thaliana* developmental transcriptome based on RNA-
766 seq profiling. *Plant J.* **88**, 1058–1070 (2016).

767 15. N. Uchida *et al.*, Chemical hijacking of auxin signaling with an engineered auxin–TIR1 pair.
768 *Nat. Chem. Biol.* **14**, 299–305 (2018).

769 16. T. Takase *et al.*, *ydk1-D* , an auxin-responsive *GH3* mutant that is involved in hypocotyl
770 and root elongation. *Plant J.* **37**, 471–483 (2004).

771 17. L. Chen, I. C. Dodd, J. C. Theobald, A. A. Belimov, W. J. Davies, , The rhizobacterium
772 *Variovorax paradoxus* 5C-2, containing ACC deaminase, promotes growth and
773 development of Arabidopsis thaliana via an ethylene-dependent pathway. *J. Exp. Bot.* **64**,
774 1565–1573 (2013).

775 18. A. J. Cary, W. Liu, S. H. Howell, Cytokinin action is coupled to ethylene in its effects on the
776 inhibition of root and hypocotyl elongation in Arabidopsis thaliana seedlings. *Plant Physiol.*

107, 1075–82 (1995).

19. L. Gómez-Gómez, G. Felix, T. Boller, A single locus determines sensitivity to bacterial flagellin in Arabidopsis thaliana. *Plant J.* **18**, 277–284 (1999).

20. P. Nagpal *et al.*, AXR2 encodes a member of the Aux/IAA protein family. *Plant Physiol.* **123**, 563–74 (2000).

21. A. E. Hall, J. L. Findell, G. E. Schaller, E. C. Sisler, A. B. Bleecker, Ethylene perception by the ERS1 protein in Arabidopsis. *Plant Physiol.* **123**, 1449–58 (2000).

22. B. W. Bardoel *et al.*, Pseudomonas Evades Immune Recognition of Flagellin in Both Mammals and Plants. *PLoS Pathog.* **7**, e1002206 (2011).

23. S. L. Sun, W. L. Yang, W. W. Fang, Y. X. Zhao, L. Guo, Y. J. Dai, The Plant Growth-Promoting Rhizobacterium *Variovorax boronicumulans* CGMCC 4969 Regulates the Level of Indole-3-Acetic Acid Synthesized from Indole-3-Acetonitrile. *App. Environ. Microbiol.* **84**, 00298–18 (2018).

24. S. J. Gould, E. S. Vrba, Exaptation—a Missing Term in the Science of Form. *Paleobiology*. **8**, 4–15 (1982).

25. A. Levy *et al.*, Genomic features of bacterial adaptation to plants. *Nat. Genet.* **50**, 138–150 (2018).

26. O. M. Finkel *et al.*, The effects of soil phosphorous content on microbiota are driven by the plant phosphate starvation response. *bioRxiv*, 608133 (2019).

27. D. S. Lundberg, S. Yourstone, P. Mieczkowski, C. D. Jones, J. L. Dangl, Practical innovations for high-throughput amplicon sequencing. *Nat. Methods*. **10**, 999–1002 (2013).

28. S. M. Yourstone, D. S. Lundberg, J. L. Dangl, C. D. Jones, MT-Toolbox: improved amplicon sequencing using molecule tags. *BMC Bioinformatics*. **15**, 284 (2014).

29. N. Joshi, J. Fass, Sickle: A sliding-window, adaptive, quality-based trimming tool for FastQ files (Version 1.33) [Software]. Available at https://github.com/najoshi/sickle. (2011).

30. R. C. Edgar, Search and clustering orders of magnitude faster than BLAST. *Bioinformatics*. **26**, 2460–2461 (2010).

31. R. C. Edgar, UPARSE: highly accurate OTU sequences from microbial amplicon reads. *Nat. Methods*. **10**, 996–998 (2013).

32. Q. Wang, G. M. Garrity, J. M. Tiedje, J. R. Cole, Naive Bayesian Classifier for Rapid Assignment of rRNA Sequences into the New Bacterial Taxonomy. *Appl. Environ. Microbiol.* **73**, 5261–5267 (2007).

33. T. Z. DeSantis *et al.*, Greengenes, a chimera-checked 16S rRNA gene database and workbench compatible with ARB. *Appl. Environ. Microbiol.* **72**, 5069–72 (2006).

34. J. Oksanen *et al.*, “Package ‘vegan’” (2015).

35. M. I. Love, W. Huber, S. Anders, Moderated estimation of fold change and dispersion for RNA-seq data with DESeq2. *Genome Biol.* **15**, 550 (2014).

36. J. Schindelin *et al.*, Fiji: an open-source platform for biological-image analysis. *Nat. Methods*. **9**, 676–682 (2012).

37. Package “emmeans” Type Package Title Estimated Marginal Means, aka Least-Squares Means (2019), doi:10.1080/00031305.1980.10483031.

38. J. Logemann, J. Schell, L. Willmitzer, Improved method for the isolation of RNA from plant tissues. *Anal. Biochem.* **163**, 16–20 (1987).

39. undefined A. S, Babraham Bioinformatics - FastQC A Quality Control tool for High Throughput Sequence Data, 3–5 (2018).

40. A. M. Bolger, M. Lohse, B. Usadel, Trimmomatic: a flexible trimmer for Illumina sequence data. *Bioinformatics*. **30**, 2114–20 (2014).

41. D. Kim, B. Langmead, S. L. Salzberg, HISAT: a fast spliced aligner with low memory requirements. *Nat. Methods*. **12**, 357–60 (2015).

42. Y. Liao, G. K. Smyth, W. Shi, The Subread aligner: fast, accurate and scalable read mapping by seed-and-vote. *Nucleic Acids Res.* **41**, e108 (2013).

43. P. Ewels, M. Magnusson, S. Lundin, M. Käller, MultiQC: summarize analysis results for multiple tools and samples in a single report. *Bioinformatics*. **32**, 3047–3048 (2016).

44. T. J. Wheeler, S. R. Eddy, nhmmer: DNA homology search with profile HMMs. *Bioinformatics*. **29**, 2487–2489 (2013).

45. K. Katoh, D. M. Standley, MAFFT multiple sequence alignment software version 7: improvements in performance and usability. *Mol. Biol. Evol.* **30**, 772–80 (2013).

46. S. Capella-Gutiérrez, J. M. Silla-Martínez, T. Gabaldón, trimAl: a tool for automated alignment trimming in large-scale phylogenetic analyses. *Bioinformatics*. **25**, 1972–3 (2009).

47. M. N. Price, P. S. Dehal, A. P. Arkin, FastTree 2 – Approximately Maximum-Likelihood Trees for Large Alignments. PLoS One. **5**, e9490 (2010).

48. S. A. Gordon, R. P. Weber, Colorimetric estimation of ildoleacetic acid, *Plant Physiol*. **26**, 192–5 (1951).

49. J. Friml *et al.*, Efflux-dependent auxin gradients establish the apical–basal axis of Arabidopsis. *Nature*. **426**, 147–153 (2003).

50. R. Donoso, P. Leiva-Novoa, A. Zúñiga, T. Timmermann, G. Recabarren-Gajardo, B. González, *Appl. Environ. Microbiol.* 83, e01991-16 (2016).

51. C. Ebenau-Jehle, M. Thomas, G. Scharf, D. Kockelkorn, B. Knapp, K. Schühle, J. Heider, G. Fuchs, *J. Bacteriol.* **194**, 2894-903 (2012).

Acknowledgments: We thank Stratton Barth, Julia Shen, Ellie Wilson, May Priegel and Dilan Chudasma for technical assistance; Dale Pelletier, DOE-ORNL for strains; the Dangl lab microbiome group for useful discussions; Anna Stepanova, Jose Alonso, Javier Brumos (North Carolina State University, USA), Joseph Kieber, Jason Reed (UNC Chapel Hill), and Isaac Greenhut (University of California, Davis) for useful discussions and Derek Lundberg (Max Planck Institute for Developmental Biology, Tübingen, Germany), and Anthony Bishopp (University of Nottingham, UK) for critical comments on the manuscript. **Funding:** This work was supported by NSF INSPIRE grant IOS-1343020 and by Office of Science (BER), U.S. Department of Energy, Grant DE-SC0014395 to J.L.D. J.L.D is an Investigator of the Howard Hughes Medical Institute, supported by the HHMI. P.J.P.L.T was supported in part by the Pew Latin American Fellows Program in the Biomedical Sciences (grant number 00026198). O.M.F was supported by NIH NRSA Fellowship F32-GM117758.

862 **Competing interests:** J.L.D. is a co-founder of, and shareholder in, AgBiome LLC, a corporation
863 whose goal is to use plant-associated microbes to improve plant productivity
864
865 **Data and materials availability:**
866 The 16S amplicon sequencing data associated with this study is deposited in the NCBI SRA
867 archive under the project accession PRJNA543313. The raw transcriptomic data is deposited in
868 the Gene Expression Omnibus (GEO) under the accession GSE131158. In addition to the
869 supplementary tables, we deposited all scripts and additional data structures required to
870 reproduce the results of this study in the following GitHub repository:
871 https://github.com/isaisg/variovoraxRGI